Article

Modeling Temperature-Dependent Vibration Damping in C/SiC Fiber-Reinforced Ceramic-Matrix Composites

Longbiao Li

College of Civil Aviation, Nanjing University of Aeronautics and Astronautics, No.29 Yudao St., Nanjing 210016, China; llb451@nuaa.edu.cn; Tel.: +86-25-8489-5963

Abstract: In this paper, the temperature-dependent vibration damping in C/SiC fiber-reinforced ceramic-matrix composites (CMCs) with different fiber preforms under different vibration frequencies is investigated. A micromechanical temperature-dependent vibration damping model is developed to establish the relationship between composite damping, material properties, internal damage mechanisms, and temperature. The effects of fiber volume, matrix crack spacing, and interface properties on temperature-dependent composite vibration damping of CMCs and interface damage are analyzed. The experimental temperature-dependent composite damping of 2D and 3D C/SiC composites is predicted for different loading frequencies. The damping of the C/SiC composite increases with temperature to the peak value and then decreases with temperature. When the vibration frequency increases from f = 1 to 10 Hz, the peak value of composite damping and corresponding temperature both decrease due to the decrease of interface debonding and slip range, and the damping of 2D C/SiC is much higher than that of 3D C/SiC at temperature range from room temperature to 400 °C. When the fiber volume and interface debonding energy increase, the peak value of composite damping and the corresponding temperature decreases, mainly attributed to the decrease of interface debonding and slip range.

Keywords: ceramic-matrix composites (CMCs); C/SiC; damping; temperature-dependent; matrix cracking; interface debonding

1. Introduction

Ceramic-matrix composites (CMCs) are the candidate materials for hot section components of aerospace vehicles, high thrust-to-weight-ratio aeroengines, satellite attitude control engines, ramjets, and thermal protection systems [1,2]. However, in the above applications, there exist vibration and noise problems. Failure analysis of rockets and satellites shows that about two-thirds of the failures are related to vibration and noise, leading to reduced operational control accuracy, structural fatigue damage, and shortened safety life [3]. Therefore, studying the damping performance of CMCs and improving their reliability in the service environment of vibration and noise is an important guarantee for the safe service of CMCs in various fields [4].

Compared with metals and alloys, CMCs have many unique damping mechanisms due to their internal structure and complex damage mechanisms [5–8]. The damping properties of composites are usually much more complicated than homogenous material. Temperature, moisture, loading frequency, and wave form affect the damping of composites [9,10]. During manufacturing and service, cracks might occur in the matrix, fiber, and interface both between fiber/matrix and neighboring plies [11]. Friction slip in the interface debonding region among matrix crack space consumes energy [12]. The internal friction of CMCs is affected by fabrication method [10], interphase thickness [13], oxidation [14],

coating, and heat treatment [15,16]. Holmes and Cho [17] developed an analytical model for predicting energy dissipation of SiC/CAS-II during a cycle based on the interfacial friction slip mechanisms. The energy dissipation corresponding to each cycle depends on stress level, matrix crack spacing, and interface frictional shear stress. Li [18] investigated internal frictional behavior of C/SiC considering fiber failure and developed temperature- and time-dependent damage models for matrix cracking [19,20]. The dynamic properties extracted from vibration response of damaged composites can be used for damage monitoring, and these include natural frequencies, mode shape, and damping. Li [21] established a relationship between natural frequency, critical rotation speed, and internal damage inside CMCs. Kyriazoglou et al. [22] measured and analyzed the specific damping capacity (SDC) of composite beams in flexure before and after quasi-static loading or fatigue damage. Zhang and Hartwig [23] detected a damping plateau from fatigue cycles in epoxy composites due to energy balance between fatigue load input and damage dissipation. However, in the research mentioned above, the synergistic effects of vibration frequency and fiber preform on temperature-dependent vibration damping of fiber-reinforced CMCs was not established.

In this paper, a micromechanical vibration damping model is developed to analyze the temperature-dependent damping of C/SiC composites with different fiber preforms under different loading frequencies. The relationships between composite damping, internal damage, and temperature are established considering different material properties and damage states. The experimental temperature-dependent damping of 2D and 3D C/SiC under vibration frequencies of f = 1, 2, 5, and 10 Hz is predicted.

2. Temperature-Dependent Damping Models

When a solid vibrates, its kinetic and strain energies transform mutually. The largest strain energy, equaling the entire energy driving vibration, determines the intensities of deformation or vibration of the structure. The proportion of energy consumed during one vibration cycle is directly associated with the vibration attenuation rate, which is also known as damping. The composite damping is given by: [7]

$$\eta = \frac{U_d}{2\pi U} \tag{1}$$

where U_d and U are dissipated energy density and maximum strain energy per cycle, respectively.

For CMCs without damage, the temperature-dependent composite damping (η_a) is obtained as:

$$\eta_a(T) = \frac{E_f(T)V_f\eta_f + E_m(T)V_m\eta_m}{E_f(T)V_f + E_m(T)V_m} \tag{2}$$

where η_f and η_m denote fiber and matrix damping, respectively; V_f and V_m are the volume of fiber and matrix, respectively; and $E_f(T)$ and $E_m(T)$ are the temperature-dependent elastic modulus of fiber and matrix, respectively.

When damage occurs inside of CMCs, the effective temperature-dependent matrix elastic modulus ($\bar{E}_m(T)$) is obtained as:

$$\bar{E}_m(T) = \frac{\tau_i(T)}{V_m} \frac{1}{\frac{\tau_i(T)}{E_c(T)} + \frac{r_f}{4l_c(T)} \frac{\Delta\sigma}{E_f(T)} \left(\frac{V_m E_m(T)}{V_f E_c(T)}\right)^2} - \frac{V_f E_f(T)}{V_m} \tag{3}$$

where $\tau_i(T)$ is the temperature-dependent interface shear stress; r_f is fiber radius; $E_c(T)$ is the temperature-dependent longitudinal modulus of intact composite material; $l_c(T)$ is the temperature-dependent matrix crack spacing; and $\Delta\sigma$ is applied stress range ($\Delta\sigma = 2\sigma$).

$$\sigma_c = \sigma(1 + \sin\omega t) \tag{4}$$

where ω is a vibration frequency.

For damaged CMCs, the energy dissipation during each vibration cycle contributes to the composite damping (η_b), which is given by:

$$\eta_b(T) \;=\; \frac{U_d(T)}{2\pi U(T)} \tag{5}$$

where

$$U_d(T) \;=\; U_{d\_u}(T) + U_{d\_r}(T) \tag{6}$$

$$U(T) \;=\; U_f(T) + U_m(T) \tag{7}$$

where $U_{d\_u}(T)$ and $U_{d\_r}(T)$ are the temperature-dependent dissipated energy density upon unloading and reloading, respectively, and $U_f(T)$ and $U_m(T)$ are the temperature-dependent fiber and matrix strain energy density, respectively.

$$U_{d\_u}(T) \;=\; 2\pi r_f \tau_i(T)\left[\frac{\Delta\sigma}{V_f E_f(T)}l_y^2(T) - \frac{8}{3}\frac{E_c(T)}{V_m E_f(T)E_m(T)}\frac{\tau_i(T)}{r_f}l_y^3(T)\right] \tag{8}$$

$$U_{d\_r}(T) \;=\; 2\pi r_f \tau_i(T)\left[\frac{\Delta\sigma}{V_f E_f(T)}l_z^2(T) - \frac{8}{3}\frac{E_c(T)}{V_m E_f(T)E_m(T)}\frac{\tau_i(T)}{r_f}l_z^3(T)\right] \tag{9}$$

$$
\begin{aligned}
U_f(T) \;=\;\; & \pi r_f^2\Bigg\{\frac{\sigma^2}{V_f^2 E_f(T)}l_d(T) - 2\frac{\sigma\tau_i(T)}{r_f V_f E_f(T)}l_d^2(T) + \frac{4}{3}\frac{\tau_i^2(T)}{r_f^2 E_f(T)}l_d^3(T) + \frac{\sigma_{fo}^2(T)}{E_f(T)}\left(\frac{l_c(T)}{2} - l_d(T)\right) \\
& + \frac{2r_f \sigma_{fo}(T)}{\rho E_f(T)}\left(\frac{V_m}{V_f}\sigma_{mo}(T) - 2\frac{l_d(T)}{r_f}\tau_i(T)\right)\left(1 - \exp\left(-\rho\frac{l_c(T)/2 - l_d(T)}{r_f}\right)\right) \\
& + \frac{r_f}{2\rho E_f(T)}\left(\frac{V_m}{V_f}\sigma_{mo}(T) - 2\frac{l_d(T)}{r_f}\tau_i(T)\right)^2\left(1 - \exp\left(-2\rho\frac{l_c(T)/2 - l_d(T)}{r_f}\right)\right)\Bigg\}
\end{aligned}
\tag{10}
$$

$$
\begin{aligned}
U_m(T) \;=\;\; & \pi r_f^2\Bigg\{\frac{4}{3}\frac{V_f^2\tau_i^2(T)}{r_f^2 V_m^2 E_m(T)}l_d^3(T) + \frac{\sigma_{mo}^2}{E_m}\left(\frac{l_c(T)}{2} - l_d(T)\right) \\
& - \frac{2r_f \sigma_{mo}(T)}{\rho E_m(T)}\left(\sigma_{mo}(T) - 2\tau_i(T)\frac{V_f}{V_m}\frac{l_d(T)}{r_f}\right)\left[1 - \exp\left[-\frac{\rho(l_c(T)/2 - l_d(T))}{r_f}\right]\right] \\
& + \frac{r_f}{2\rho E_m(T)}\left(\sigma_{mo}(T) - 2\tau_i(T)\frac{V_f}{V_m}\frac{l_d(T)}{r_f}\right)^2\left[1 - \exp\left[-2\frac{\rho(l_c(T)/2 - l_d(T))}{r_f}\right]\right]\Bigg\}
\end{aligned}
\tag{11}
$$

where $l_d(T)$, $l_y(T)$, and $l_z(T)$ are temperature-dependent interface debonding length, counter slip length, and new slip length, respectively; ρ is shear-lag model parameter; and $\sigma_{fo}(T)$ and $\sigma_{mo}(T)$ are temperature-dependent fiber and matrix axial stress in the interface bonding region, respectively.

$$l_d(T) \;=\; \frac{r_f}{2}\left(\frac{V_m E_m(T)\sigma}{V_f E_c(T)\tau_i(T)} - \frac{1}{\rho}\right) - \sqrt{\left(\frac{r_f}{2\rho}\right)^2 + \frac{r_f V_m E_m(T)E_f(T)}{E_c(T)\tau_i^2(T)}\xi_d(T)} \tag{12}$$

$$l_y(T) \;=\; \frac{1}{2}\left\{l_d(T) - \left[\frac{r_f}{2}\left(\frac{V_m E_m(T)\sigma}{V_f E_c(T)\tau_i(T)} - \frac{1}{\rho}\right) - \sqrt{\left(\frac{r_f}{2\rho}\right)^2 + \frac{r_f V_m E_m(T)E_f(T)}{E_c(T)\tau_i^2(T)}\xi_d(T)}\right]\right\} \tag{13}$$

$$l_z(T) \;=\; l_y(T) - \frac{1}{2}\left\{l_d(T) - \left[\frac{r_f}{2}\left(\frac{V_m E_m(T)\sigma}{V_f E_c(T)\tau_i(T)} - \frac{1}{\rho}\right) - \sqrt{\left(\frac{r_f}{2\rho}\right)^2 + \frac{r_f V_m E_m(T)E_f(T)}{E_c(T)\tau_i^2(T)}\xi_d(T)}\right]\right\} \tag{14}$$

$$\sigma_{fo}(T) \;=\; \frac{E_f(T)}{E_c(T)}\sigma + E_f(T)(\alpha_{lc}(T) - \alpha_{lf}(T))\Delta T \tag{15}$$

$$\sigma_{mo}(T) \;=\; \frac{E_m(T)}{E_c(T)}\sigma + E_m(T)(\alpha_{lc}(T) - \alpha_{lm}(T))\Delta T \tag{16}$$

where $\xi_d(T)$ denotes temperature-dependent interface debonding energy; $\alpha_{lf}(T)$, $\alpha_{lm}(T)$, and $\alpha_{lc}(T)$ are temperature-dependent fiber, matrix, and composite axial thermal expansion coefficient, respectively; and ΔT denotes temperature difference between testing temperature (T) and fabricated temperature (T_0).

The total temperature-dependent composite damping (η_c) can be determined as:

$$\eta_c = \eta_a + \eta_b \tag{17}$$

where η_a and η_b can be determined by Equations (2) and (5), respectively.

3. Results and Discussion

The material properties of the C/SiC composite are given by: $V_f = 0.3$, $r_f = 3.5$ μm, $\xi_d = 0.1$ J/m^2, $\eta_f = 0.002$, $\eta_m = 0.001$, and $T_0 = 1000$ °C, and the temperature-dependent constituent properties are given by [24–28]:

$$E_f(T) = 230\left[1 - 2.86 \times 10^{-4}\exp\left(\frac{T+273}{324}\right)\right], T < 2000\ °C \tag{18}$$

$$E_m(T) = \frac{350}{460}\left[460 - 0.04(T+273)\exp\left(-\frac{962}{T+273}\right)\right], T \in \left[27°C,\ 1500\ °C\right] \tag{19}$$

$$\alpha_{lf}(T) = 2.529 \times 10^{-2} - 1.569 \times 10^{-4}(T+273) + 2.228 \times 10^{-7}(T+273)^2$$
$$-1.877 \times 10^{-11}(T+273)^3 - 1.288 \times 10^{-14}(T+273)^4, T \in \left[27°C,\ 2227\ °C\right] \tag{20}$$

$$\alpha_{rf}(T) = -1.86 \times 10^{-1} + 5.85 \times 10^{-4}(T+273) - 1.36 \times 10^{-8}(T+273)^2$$
$$+1.06 \times 10^{-22}(T+273)^3, T \in \left[27°C,\ 2500\ °C\right] \tag{21}$$

$$\alpha_{lm}(T) = \alpha_{rm}(T) = \begin{cases} -1.8276 + 0.0178(T+273) - 1.5544 \times 10^{-5}(T+273)^2 \\ \qquad\qquad +4.5246 \times 10^{-9}(T+273)^3, \quad T \in \left[0°C,\ 1000\ °C\right] \\ 5.0 \times 10^{-6}, \quad T > 1000\ °C \end{cases} \tag{22}$$

$$\tau_i(T) = \tau_0 + \mu\frac{|\alpha_{rf}(T) - \alpha_{rm}(T)|(T_0 - T)}{A} \tag{23}$$

where τ_0 is the steady-state interface shear stress; μ is the interface frictional coefficient; α_{rf} and α_{rm} denote the temperature-dependent fiber and matrix radial thermal expansion coefficient, respectively; and A is a constant depending on the elastic properties of the matrix and the fiber.

$$\xi_d(T) = \xi_{dr}\left[1 - \frac{\int_{T_r}^{T} C_P(T)dT}{\int_{T_r}^{T_0} C_P(T)dT}\right] \tag{24}$$

where T_r denotes the reference temperature; T_0 denotes the fabricated temperature; and ξ_{dr} denotes the interface debonding energy at the reference temperature of T_r.

The effects of material properties and damage state on temperature-dependent composite damping and interface damage of the C/SiC composite are analyzed.

3.1. Effect of Fiber Volume on Temperature-Dependent Damping of C/SiC Composite

The effect of fiber volume ($V_f = 30\%$ and 35%) on temperature-dependent composite damping (η_c), interface debonding, and slip length ($2l_d/l_c$, $2l_y/l_c$) versus temperature curves of the C/SiC composite is analyzed for the temperature range from room temperature ($T = 20$ °C) to elevated temperature of $T = 400$ °C, as shown in Figure 1 and Table 1.
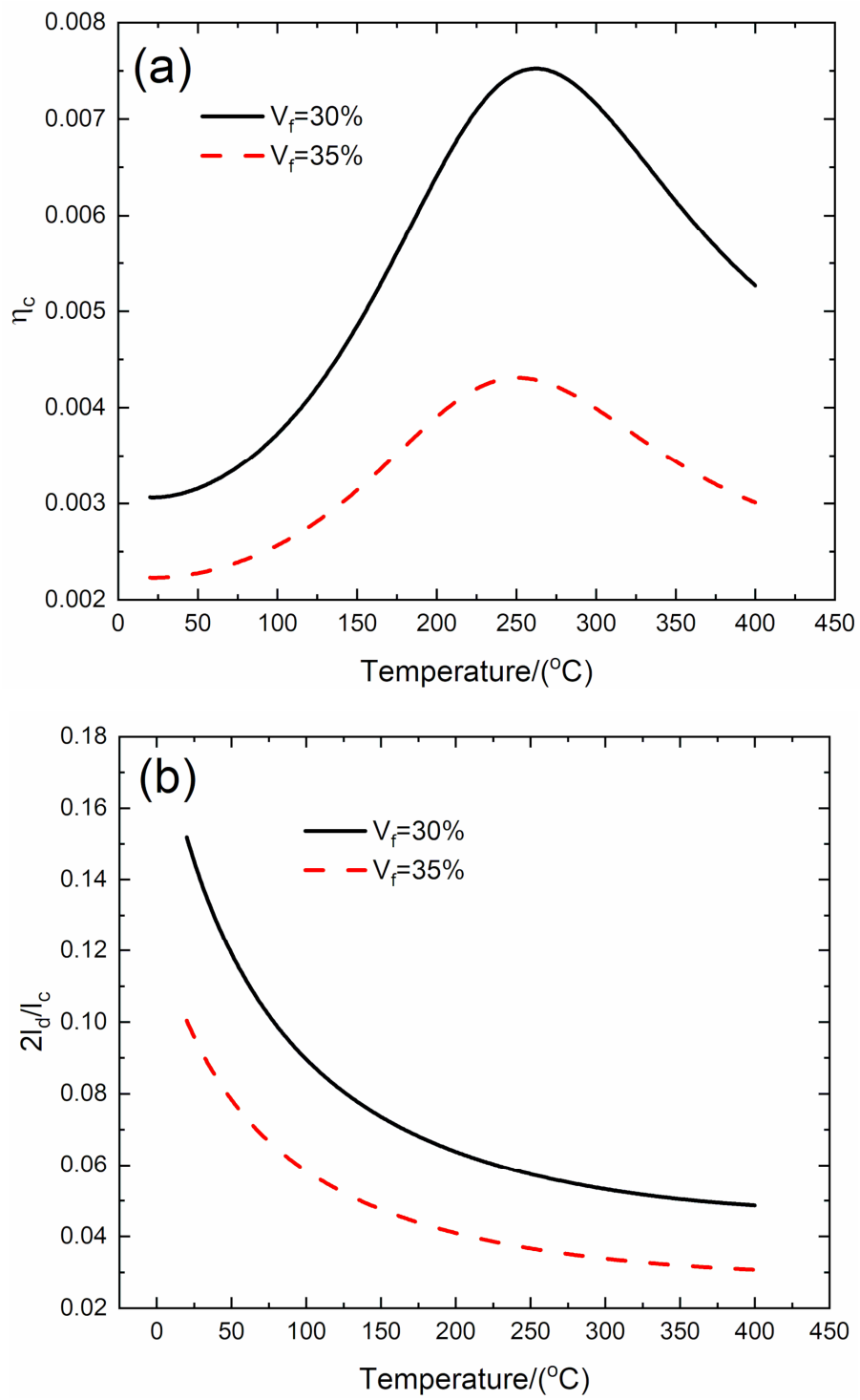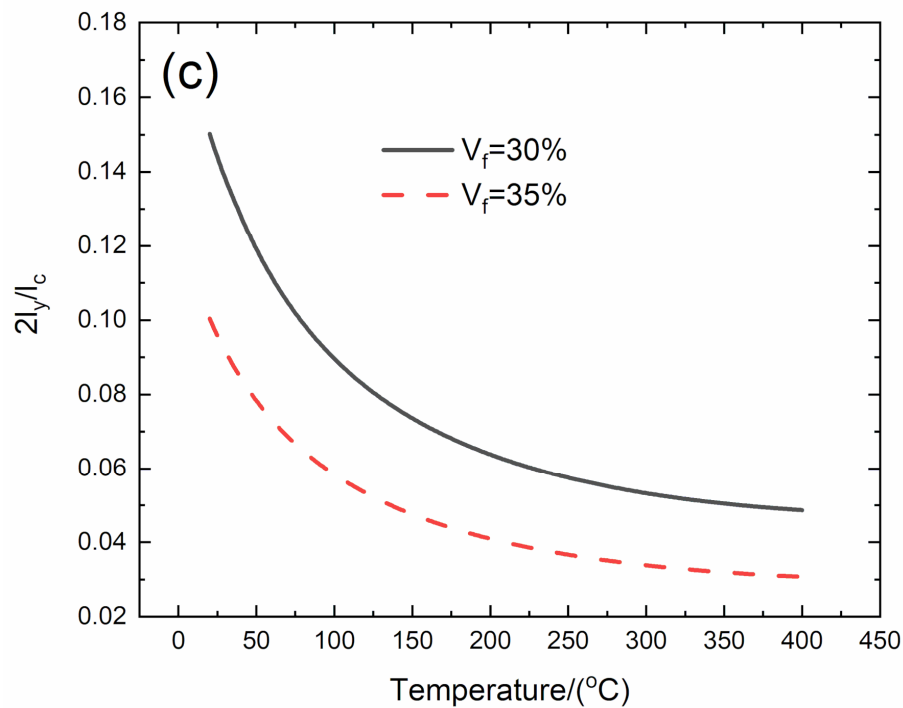
Figure 1. *Cont.*

Figure 1. Effect of fiber volume (V_f = 30% and 35%) on (**a**) the temperature-dependent composite damping (η_c) versus temperature curves; (**b**) the temperature-dependent interface debonding length ($2l_d/l_c$) versus temperature curves; and (**c**) the temperature-dependent interface slip length ($2l_y/l_c$) versus temperature curves of C/SiC composite.

Table 1. Temperature-dependent composite damping, interface debonding, and slip length of C/SiC composite for different fiber volumes.

	$T/(°C)$	η_c	$2l_d/l_c$	$2l_y/l_c$
	20	0.00306	0.152	0.15
$V_f = 30\%$	262	0.00752	0.056	0.056
	400	0.00527	0.048	0.048
	$T/(°C)$	η_c	$2l_d/l_c$	$2l_y/l_c$
	20	0.00223	0.1	0.1
$V_f = 35\%$	250	0.00431	0.036	0.036
	400	0.00301	0.03	0.03

When V_f = 30%, the temperature-dependent composite damping (η_c) increases from η_c = 0.00306 at T = 20 °C to peak value η_c = 0.00752 at T = 262 °C and decreases to η_c = 0.00527 at T = 400 °C; the temperature-dependent interface debonding length ($2l_d/l_c$) decreases from $2l_d/l_c$ = 0.152 at T = 20 °C to $2l_d/l_c$ = 0.048 at T = 400 °C; and the temperature-dependent interface slip length ($2l_y/l_c$) decreases from $2l_y/l_c$ = 0.15 at T = 20 °C to $2l_y/l_c$ = 0.048 at T = 400 °C.

When V_f = 35 %, the temperature-dependent composite damping (η_c) increases from η_c = 0.00223 at T = 20 °C to peak value η_c = 0.00431 at T = 250 °C, and decreases to η_c = 0.00301 at T = 400 °C; the temperature-dependent interface debonding length ($2l_d/l_c$) decreases from $2l_d/l_c$ = 0.1 at T = 20 °C to $2l_d/l_c$ = 0.03 at T = 400 °C; and the temperature-dependent interface slip length ($2l_y/l_c$) decreases from $2l_y/l_c$ = 0.1 at T = 20 °C to $2l_y/l_c$ = 0.03 at T = 400 °C.

At the temperature range from room temperature (T = 20 °C) to elevated temperature of T = 400 °C, the temperature-dependent composite damping of the C/SiC composite increases with temperature to the peak value first and then decreases with temperature. When the fiber volume increases from

V_f = 30% to 35%, the temperature-dependent peak value damping of the C/SiC composite (η_c) decreases from η_c = 0.00752 to η_c = 0.00431, and the corresponding temperature for the peak value damping of the C/SiC composite decreases from T = 262 °C to T = 250 °C, mainly attributed to the decrease of interface debonding and slip length.

3.2. Effect of Matrix Crack Spacing on Temperature-Dependent Damping of C/SiC Composite

The effect of matrix crack spacing (l_c = 300 and 400 μm) on temperature-dependent composite damping (η_c), interface debonding, and slip length ($2l_d/l_c$, $2l_y/l_c$) versus temperature curves of the C/SiC composite is analyzed for the temperature range from room temperature (T = 20 °C) to elevated temperature of T = 400 °C, as shown in Figure 2 and Table 2.
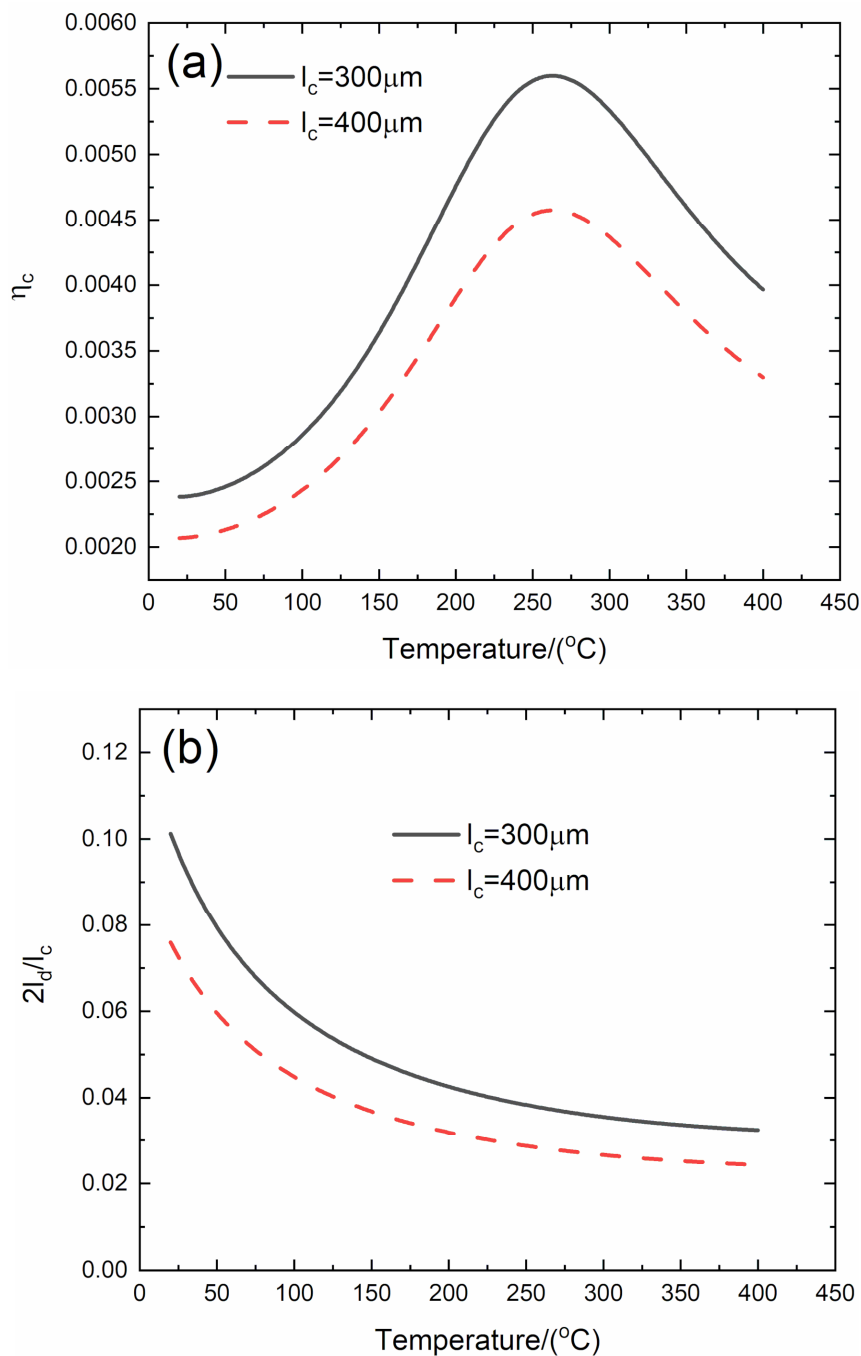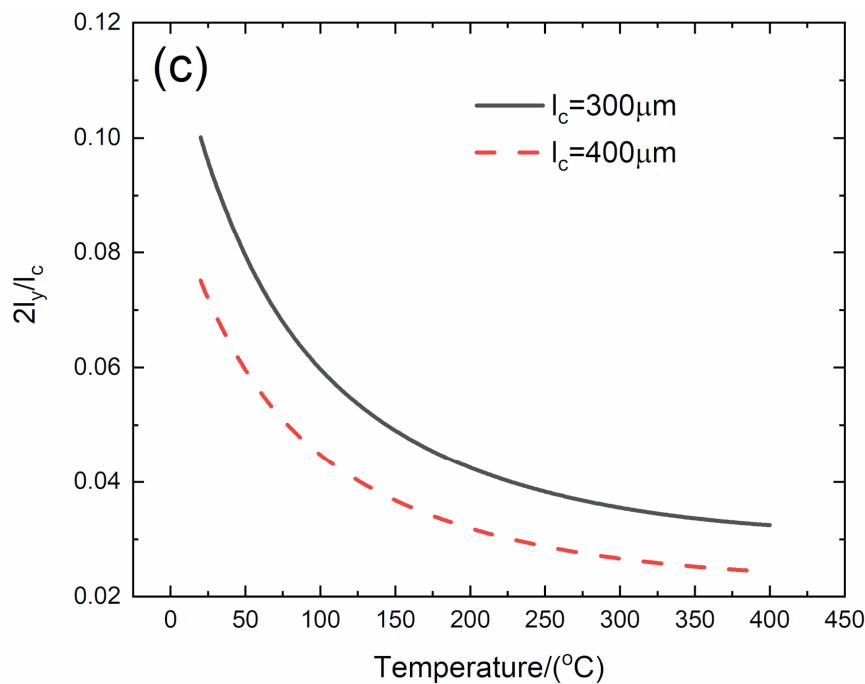

Figure 2. *Cont.*

Figure 2. Effect of matrix crack spacing (l_c = 300 and 400 µm) on (**a**) the temperature-dependent composite damping (η_c) versus temperature curves; (**b**) the temperature-dependent interface debonding length ($2l_d/l_c$) versus temperature curves; and (**c**) the temperature-dependent interface slip length ($2l_y/l_c$) versus temperature curves of C/SiC composite.

Table 2. Temperature-dependent composite damping, interface debonding, and slip length of C/SiC composite for different matrix crack spacing.

	$T/(°C)$	η_c	$2l_d/l_c$	$2l_y/l_c$
	20	0.00238	0.101	0.1
l_c = 300µm	263	0.0056	0.037	0.037
	400	0.0039	0.032	0.032
	$T/(°C)$	η_c	$2l_d/l_c$	$2l_y/l_c$
	20	0.00207	0.0759	0.0751
l_c = 400µm	263	0.00458	0.0281	0.0281
	400	0.00207	0.0243	0.0243

When l_c = 300 µm, the temperature-dependent composite damping (η_c) increases from η_c = 0.00238 at T = 20 °C to peak value η_c = 0.0056 at T = 263 °C and decreases to η_c = 0.00397 at T = 400 °C; the temperature-dependent interface debonding length ($2l_d/l_c$) decreases from $2l_d/l_c$ = 0.101 at T = 20 °C to $2l_d/l_c$ = 0.032 at T = 400 °C; and the temperature-dependent interface slip length ($2l_y/l_c$) decreases from $2l_y/l_c$ = 0.1 at T = 20 °C to $2l_y/l_c$ = 0.032 at T = 400 °C.

When l_c = 400 µm, the temperature-dependent composite damping (η_c) increases from η_c = 0.00207 at T = 20 °C to peak value η_c = 0.00458 at T = 263 °C and decreases to η_c = 0.00207 at T = 400 °C; the temperature-dependent interface debonding length ($2l_d/l_c$) decreases from $2l_d/l_c$ = 0.0759 at T = 20 °C to $2l_d/l_c$ = 0.0243 at T = 400 °C; and the temperature-dependent interface slip length ($2l_y/l_c$) decreases from $2l_y/l_c$ = 0.0751 at T = 20 °C to $2l_y/l_c$ =0.0243 at T = 400 °C.

When matrix crack spacing increases from l_c = 300 to 400 µm, the peak damping of the C/SiC composite decreases from η_c = 0.0056 to η_c = 0.00458, and the interface debonding and slip length at the same temperature also decrease.

3.3. Effect of Interface Debonding Energy on Temperature-Dependent Damping of C/SiC Composite

The effect of interface debonding energy (ξ_d = 0.2 and 0.3 J/m^2) on temperature-dependent composite damping (η_c), interface debonding, and slip length ($2l_d/l_c$, $2l_y/l_c$) versus temperature curves of the C/SiC composite is analyzed for the temperature range from room temperature (T = 20 °C) to elevated temperature of T = 400 °C, as shown in Figure 3 and Table 3.
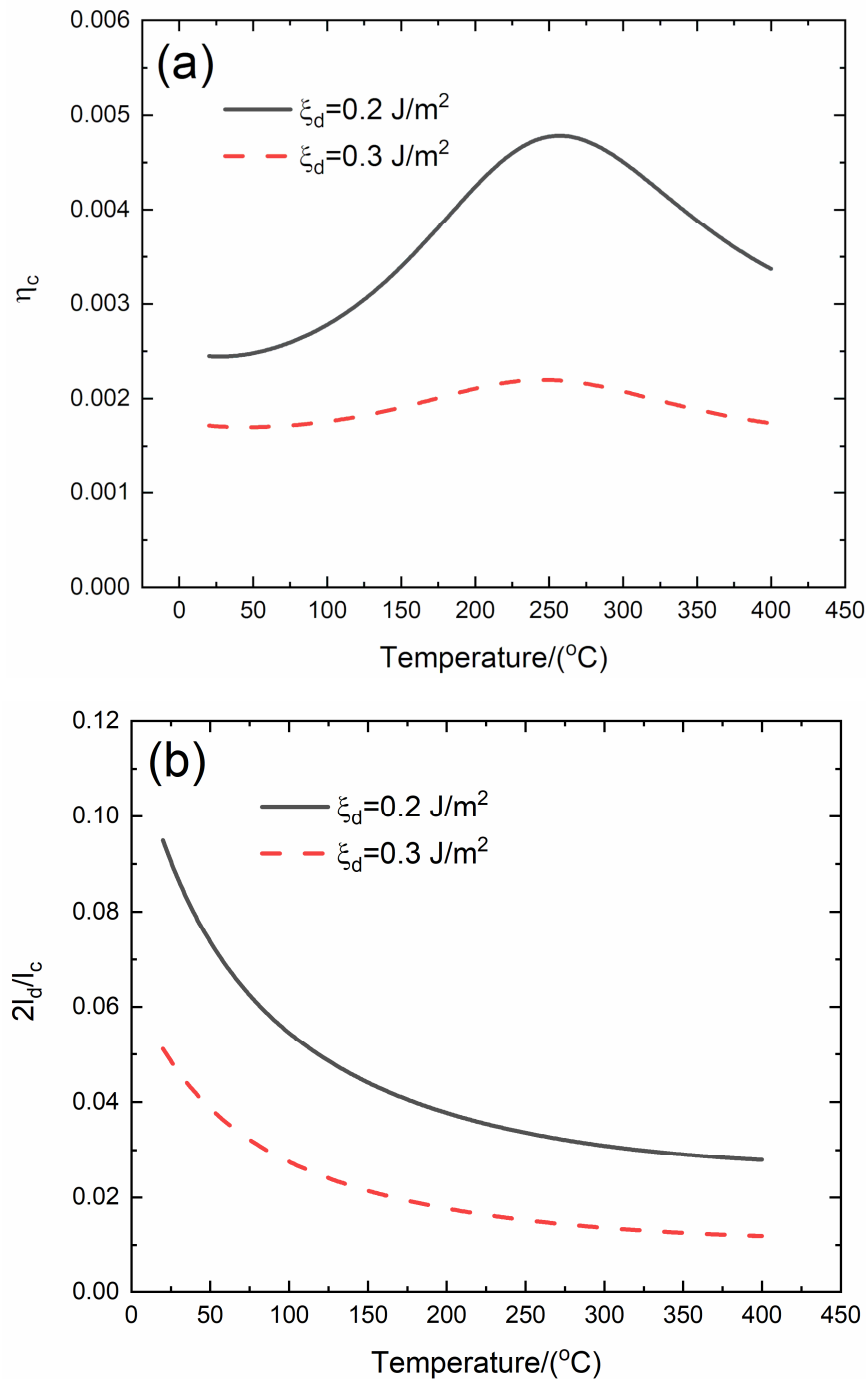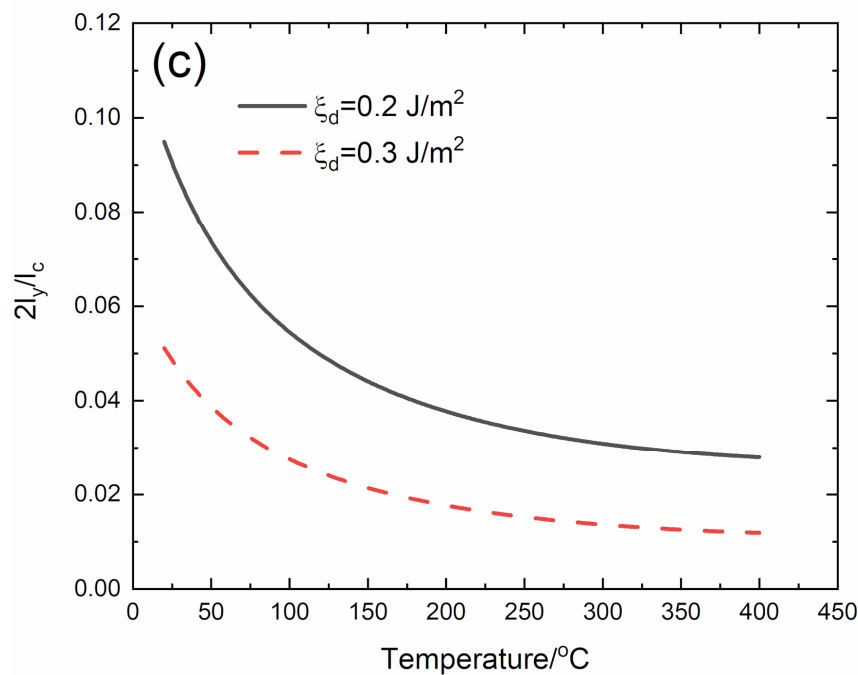

Figure 3. *Cont.*

Figure 3. Effect of interface debonding energy (ξ_d = 0.2 and 0.3 J/m²) on (**a**) the temperature-dependent composite damping (η_c) versus temperature curves; (**b**) the temperature-dependent interface debonding length ($2l_d/l_c$) versus temperature curves; and (**c**) the temperature-dependent interface slip length ($2l_y/l_c$) versus temperature curves of C/SiC composite.

Table 3. Temperature-dependent composite damping, interface debonding, and slip length of C/SiC composite for different interface debonding energy.

	$T/(°C)$	η_c	$2l_d/l_c$	$2l_y/l_c$
	20	0.00245	0.0949	0.0949
ξ_d = 0.2 J/m²	256	0.00478	0.0332	0.0332
	400	0.00337	0.0279	0.0279
	$T/(°C)$	η_c	$2l_d/l_c$	$2l_y/l_c$
	20	0.00172	0.0511	0.0511
ξ_d = 0.3 J/m²	245	0.0022	0.0154	0.0154
	400	0.00174	0.0118	0.0118

When ξ_d = 0.2 J/m², the temperature-dependent composite damping (η_c) increases from η_c = 0.00245 at T = 20 °C to peak value η_c = 0.00478 at T = 256 °C and decreases to η_c = 0.00337 at T = 400 °C; the temperature-dependent interface debonding length ($2l_d/l_c$) decreases from $2l_d/l_c$ = 0.0949 at T = 20 °C to $2l_d/l_c$ = 0.0279 at T = 400 °C; and the temperature-dependent interface slip length ($2l_y/l_c$) decreases from $2l_y/l_c$ = 0.0949 at T = 20 °C to $2l_y/l_c$ = 0.0279 at T = 400 °C.

When ξ_d = 0.3 J/m², the temperature-dependent composite damping (η_c) increases from η_c = 0.00172 at T = 20 °C to peak value η_c = 0.0022 at T = 245 °C and then decreases to η_c = 0.00174 at T = 400 °C; the temperature-dependent interface debonding length ($2l_d/l_c$) decreases from $2l_d/l_c$ = 0.0511 at T = 20 °C to $2l_d/l_c$ = 0.0118 at T = 400 °C; and the temperature-dependent interface slip length ($2l_y/l_c$) decreases from $2l_y/l_c$ = 0.0511 at T = 20 °C to $2l_y/l_c$ = 0.0118 at T = 400 °C.

When interface debonding energy increases from ξ_d = 0.2 to 0.3 J/m², the peak damping of the C/SiC composite decreases from η_c = 0.00478 to η_c = 0.0022, and the corresponding temperature for peak damping decreases from T = 256 to T = 245 °C, and the interface debonding and slip length at the same temperature also decrease.

3.4. Effect of Steady-State Interface Shear Stress on Temperature-Dependent Damping of C/SiC Composite

The effect of steady-state interface shear stress (τ_0 = 40 and 50 MPa) on temperature-dependent composite damping (η_c), interface debonding, and slip length ($2l_d/l_c$, $2l_y/l_c$), and interface slip length versus temperature curves of the C/SiC composite are analyzed for the temperature range from room temperature (T = 20 °C) to elevated temperature of T = 400 °C, as shown in Figure 4 and Table 4.
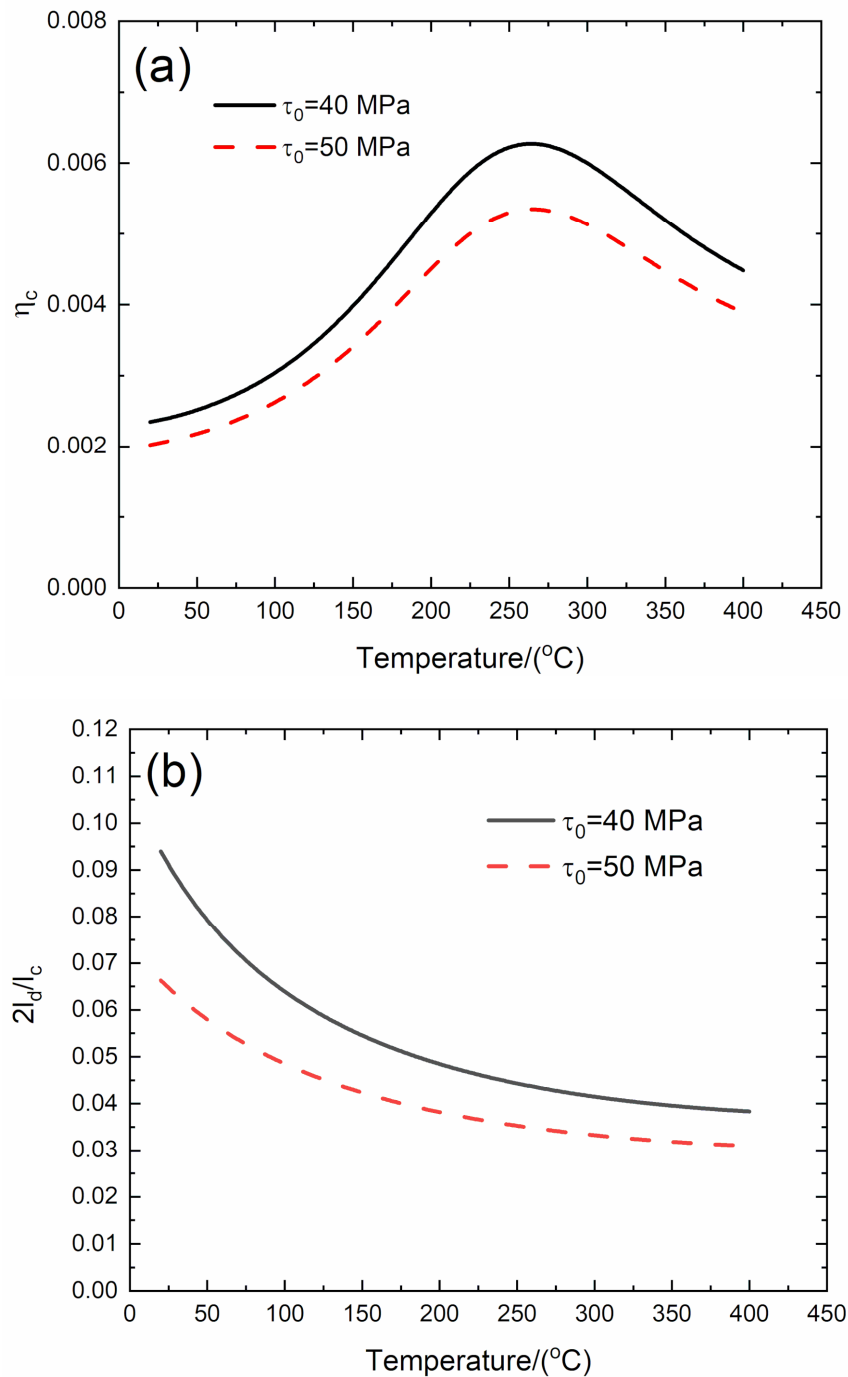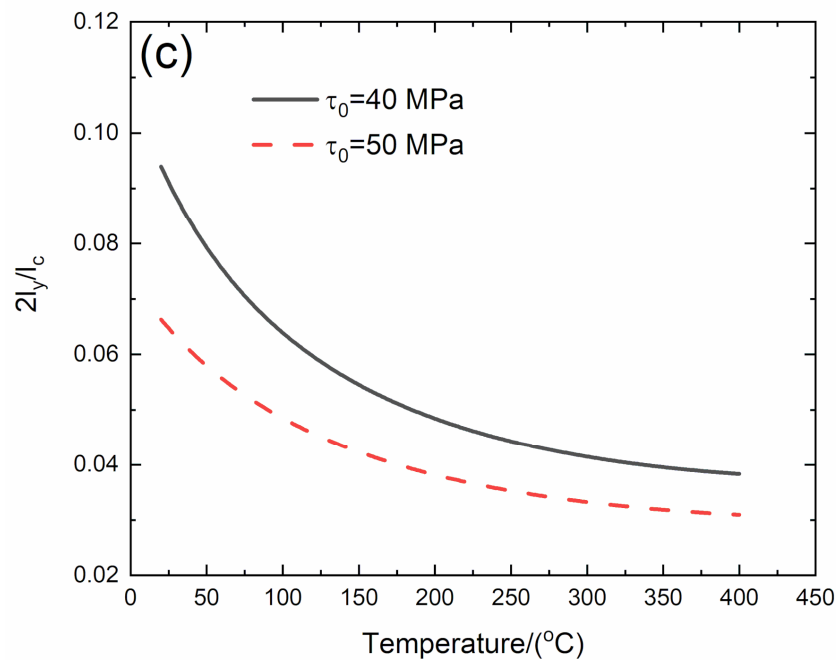

Figure 4. *Cont.*

Figure 4. Effect of steady-state interface shear stress (τ_0 = 40 and 50 MPa) on (**a**) the temperature-dependent composite damping (η_c) versus temperature curves; (**b**) the temperature-dependent interface debonding length ($2l_d/l_c$) versus temperature curves; and (**c**) the temperature-dependent interface slip length ($2l_y/l_c$) versus temperature curves of C/SiC composite.

Table 4. Temperature-dependent composite damping, interface debonding, and slip length of C/SiC composite for different steady-state interface shear stress.

	$T/(°C)$	η_c	$2l_d/l_c$	$2l_y/l_c$
	20	0.00235	0.094	0.094
τ_0 =4 0 MPa	264	0.00627	0.043	0.043
	400	0.00448	0.038	0.038
	$T/(°C)$	η_c	$2l_d/l_c$	$2l_y/l_c$
	20	0.00202	0.0663	0.0663
τ_0 = 50 MPa	265	0.00535	0.0345	0.0345
	400	0.00389	0.0309	0.0309

When τ_0 = 40 MPa, the temperature-dependent composite damping (η_c) increases from η_c = 0.00235 at T = 20 °C to peak value η_c = 0.00627 at T = 264 °C and decreases to η_c = 0.00448 at T = 400 °C; the interface debonding length ($2l_d/l_c$) decreases from $2l_d/l_c$ = 0.094 at T = 20 °C to $2l_d/l_c$ = 0.038 at T = 400 °C; and the interface slip length ($2l_y/l_c$) decreases from $2l_y/l_c$ = 0.094 at T = 20 °C to $2l_y/l_c$ = 0.038 at T = 400 °C.

When τ_0 = 50 MPa, the temperature-dependent composite damping (η_c) increases from η_c = 0.00202 at T = 20 °C to peak value η_c = 0.00535 at T = 265 °C and decreases to η_c = 0.00389 at T = 400 °C; the temperature-dependent interface debonding length ($2l_d/l_c$) decreases from $2l_d/l_c$ = 0.0663 at T = 20 °C to $2l_d/l_c$ = 0.0309 at T = 400 °C; and the temperature-dependent interface slip length ($2l_y/l_c$) decreases from $2l_y/l_c$ = 0.0663 at T = 20 °C to $2l_y/l_c$ = 0.0309 at T = 400 °C.

When the steady-state interface shear stress increases from τ_0 = 40 to 50 MPa, the peak damping of the C/SiC composite decreases from η_c = 0.00627 to η_c = 0.00535, and the interface debonding and slip length at the same temperature also decrease.

4. Experimental Comparisons

Wang et al. [15] investigated damping capacity of 2D and 3D T-300[TM] C/SiC composites at different vibration frequencies. The 2D C/SiC composite is prepared by laminating 1K T-300 woven carbon fabrics, and the 3D C/SiC composite is prepared by braiding 3K T-300 carbon fibers in a four-step method. The volume of fiber was about 40% and the fiber diameter is 7.0 μm. The C/SiC with the PyC interphase was fabricated using chemical vapor infiltration (CVI). The deposition conditions of PyC interlayer were as follows: temperature 960 °C, pressure 5 kPa, Ar flow 200 ml/min, and butane flow 15 ml/min. The infiltration conditions of the SiC matrix were as follows: temperature 1000 °C, pressure 5 kPa, time 120 h, H_2 flow 350 ml/min, Ar flow 350 ml/min, and molar ratio of H_2 and MTS 10. A Dynamical Mechanical Analyzer (DMA 2980) made by TA company, USA, was used for damping measurements of the C/SiC composite. All of the measurements were performed in air atmosphere from room temperature to 400 °C, and the testing frequencies were f = 1, 2, 5, and 10 Hz.

4.1. 2D C/SiC Composite

4.1.1. f = 1 Hz

The experimental and predicted temperature-dependent composite damping (η_c), interface debonding, and slip length ($2l_d/l_c$, $2l_y/l_c$) versus temperature curves of the 2D C/SiC composite at the vibration frequency of f = 1 Hz are shown in Figure 5 and Table 5. The predicted peak composite damping agrees with experimental data, and the predicted corresponding temperature for peak composite damping is a little lower than the experimental data.
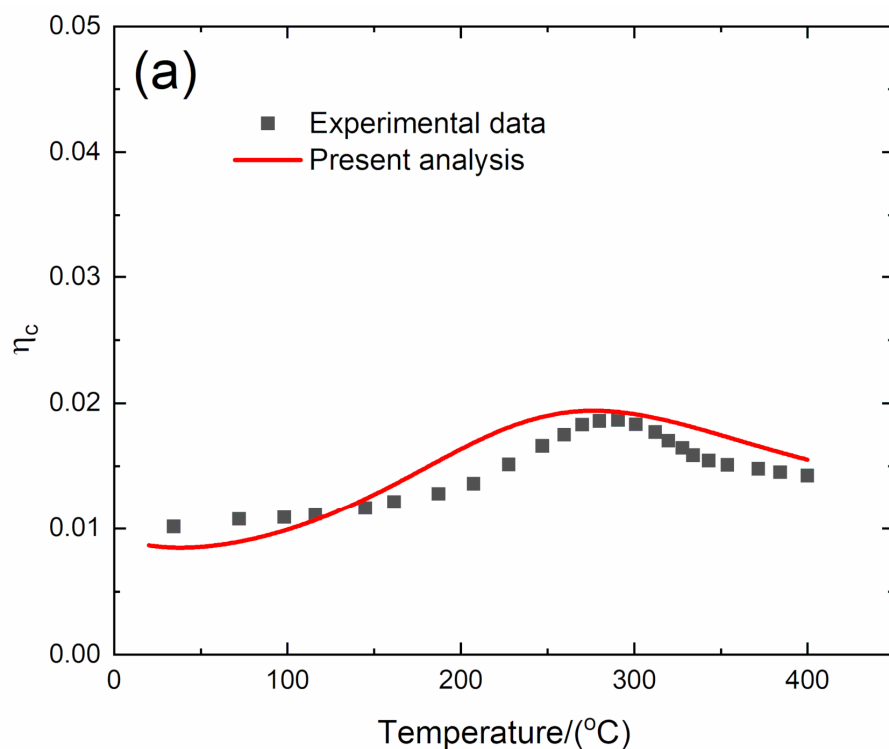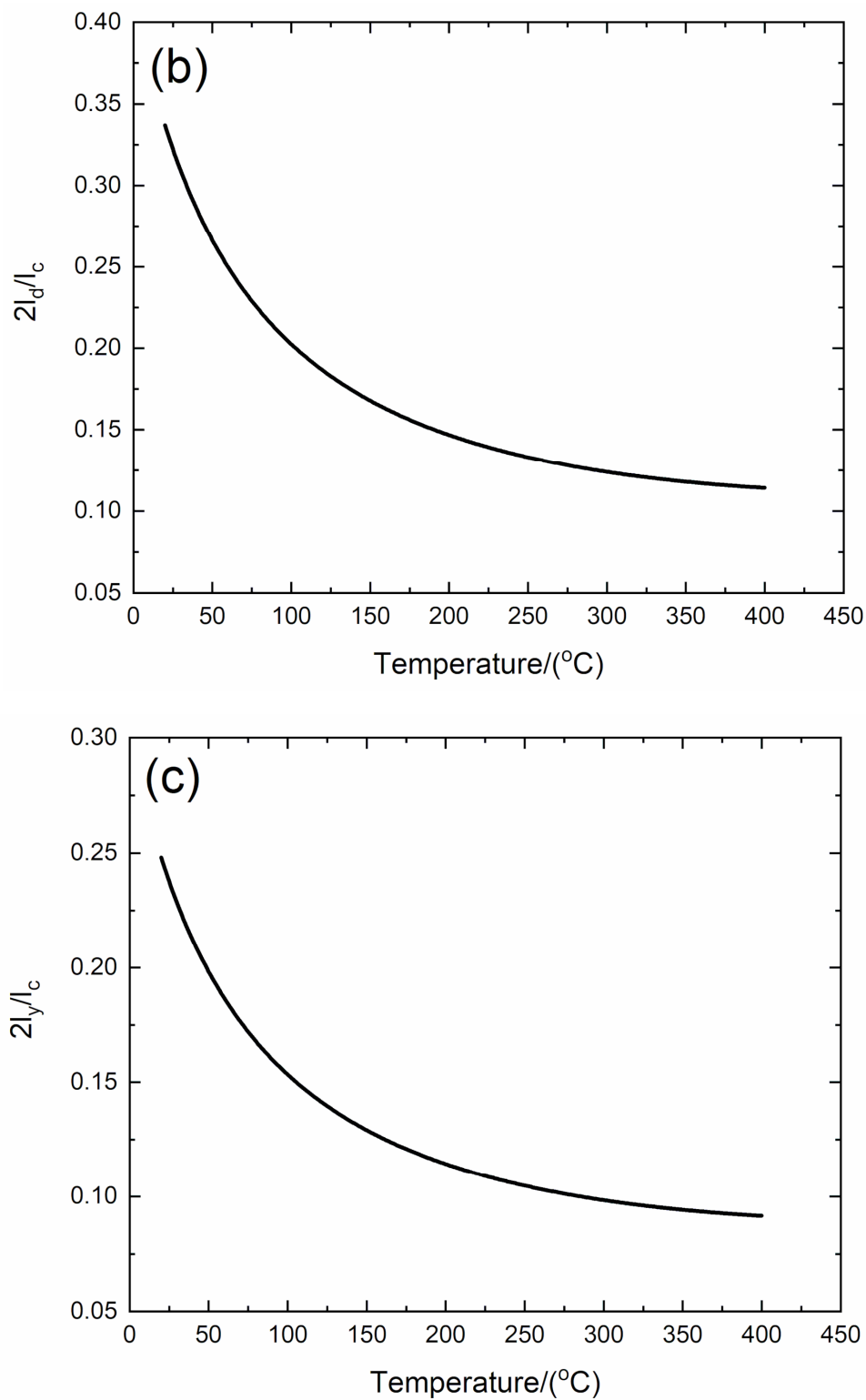

Figure 5. *Cont.*

Figure 5. (**a**) Experimental and predicted temperature-dependent composite damping (η_c) versus temperature curves; (**b**) the temperature-dependent interface debonding length ($2l_d/l_c$) versus temperature curves; and (**c**) the temperature-dependent interface slip length ($2l_y/l_c$) versus temperature curves of 2D C/SiC composite at the vibration frequency of f = 1 Hz.

Table 5. Experimental and predicted peak value of composite damping and corresponding temperature of 2D C/SiC composite under the vibration frequencies of f = 1, 2, 5, and 10 Hz at temperature range from room temperature to 400 °C.

Frequency/Hz	Experiment [15]		Theory	
	Peak Damping	**Temperature/(°C)**	**Peak Damping**	**Temperature/(°C)**
1	0.019	283	0.019	279
2	0.015	266	0.014	283
5	0.0106	261	0.0101	263
10	0.010	258	0.0095	256

The experimental composite damping increases from $\eta_c = 0.01$ at room temperature to peak value of $\eta_c = 0.019$ at temperature of $T = 283$ °C and then decreases to $\eta_c = 0.014$ at temperature of $T = 400$ °C. The theoretical predicted composite damping increases from $\eta_c = 0.008$ at room temperature to peak value $\eta_c = 0.019$ at temperature of $T = 279$ °C and then decreases to $\eta_c = 0.015$ at temperature of $T = 400$ °C. The interface debonding length ($2l_d/l_c$) decreases from $2l_d/l_c = 0.337$ at room temperature to $2l_d/l_c = 0.114$ at temperature of $T = 400$ °C, and the interface slip length ($2l_y/l_c$) decreases from $2l_y/l_c = 0.248$ at room temperature to $2l_y/l_c = 0.091$ at temperature of $T = 400$ °C.

4.1.2. $f = 2$ Hz

The experimental and predicted temperature-dependent composite damping (η_c), interface debonding, and slip length ($2l_d/l_c$, $2l_y/l_c$) versus temperature curves of the 2D C/SiC composite at the vibration frequency of $f = 2$ Hz are shown in Figure 6 and Table 5.
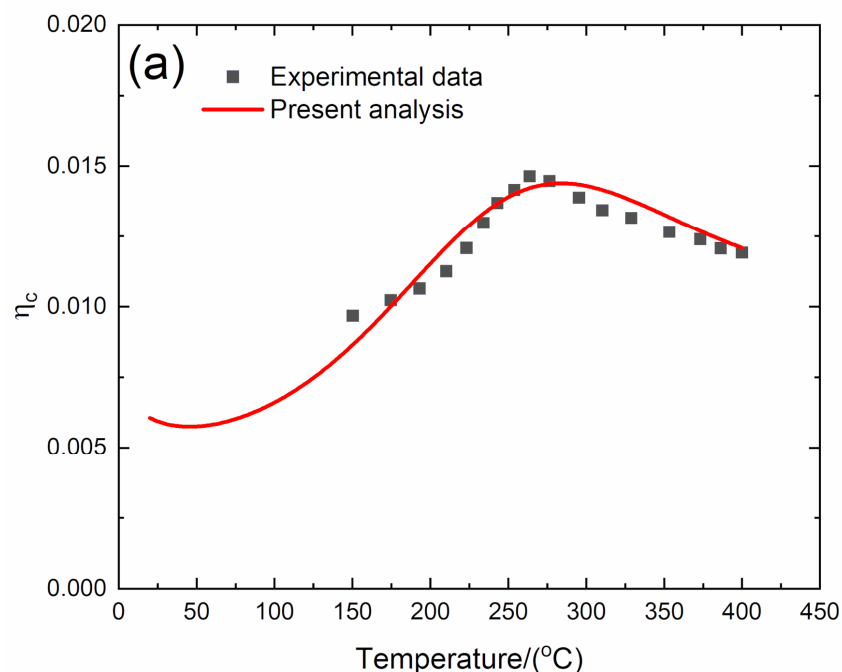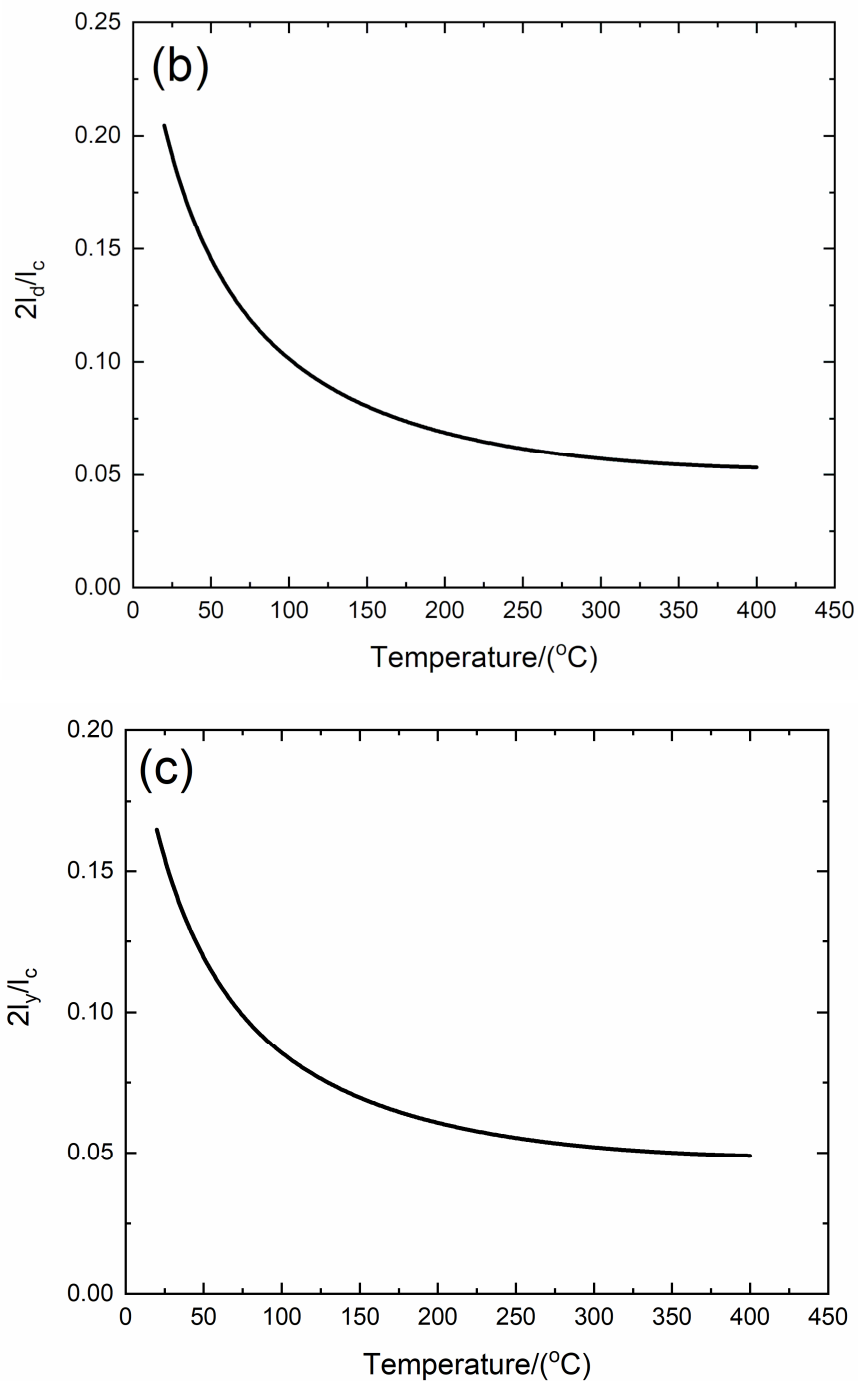

Figure 6. *Cont.*

Figure 6. (**a**) Experimental and predicted temperature-dependent composite damping (η_c) versus temperature curves; (**b**) the temperature-dependent interface debonding length ($2l_d/l_c$) versus temperature curves; and (**c**) the temperature-dependent interface slip length ($2l_y/l_c$) versus temperature curves of 2D C/SiC composite at the vibration frequency of $f = 2$ Hz.

The experimental composite damping (η_c) increases from $\eta_c = 0.009$ at temperature of $T = 150\ ^\circ\text{C}$ to the peak value of $\eta_c = 0.015$ at temperature of $T = 266\ ^\circ\text{C}$ and then decreases to $\eta_c = 0.012$ at temperature of $T = 400\ ^\circ\text{C}$. The theoretical predicted composite damping increases from $\eta_c = 0.006$ at room temperature to the peak value of $\eta_c = 0.0144$ at temperature of $T = 283\ ^\circ\text{C}$ and then decreases to $\eta_c = 0.012$ at temperature of $T = 400\ ^\circ\text{C}$. The interface debonding length ($2l_d/l_c$) decreases from $2l_d/l_c = 0.2$ at room temperature to $2l_d/l_c = 0.05$ at temperature of $T = 400\ ^\circ\text{C}$, and the interface slip

length ($2l_y/l_c$) decreases from $2l_y/l_c = 0.16$ at room temperature to $2l_y/l_c = 0.048$ at temperature of $T = 400\,°C$.

4.1.3. $f = 5$ Hz

The experimental and predicted temperature-dependent composite damping (η_c), interface debonding, and slip length ($2l_d/l_c$, $2l_y/l_c$) versus temperature curves of the 2D C/SiC composite at the vibration frequency of $f = 5$ Hz are shown in Figure 7 and Table 5.
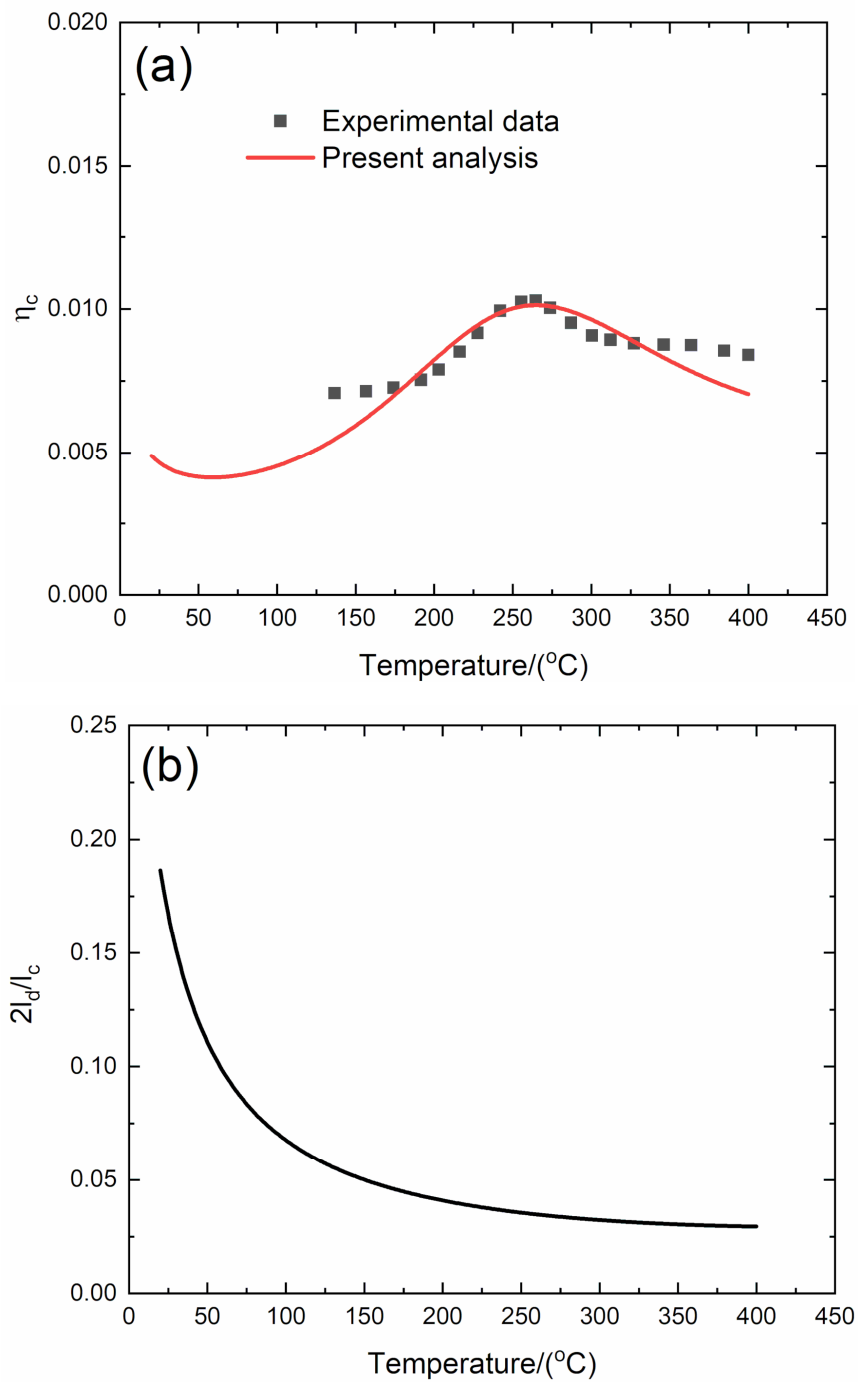

Figure 7. *Cont.*
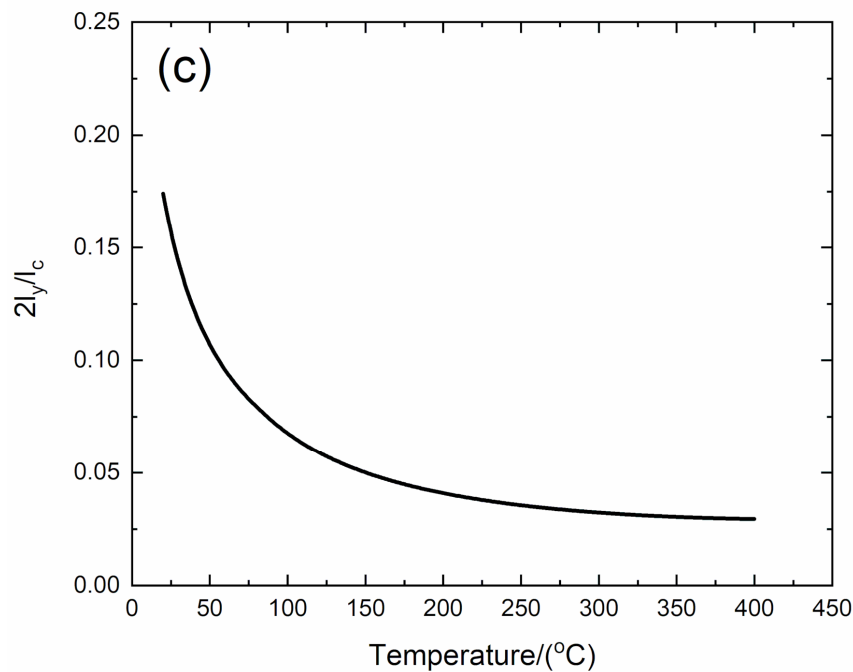
Figure 7. (**a**) Experimental and predicted temperature-dependent composite damping (η_c) versus temperature curves; (**b**) the temperature-dependent interface debonding length ($2l_d/l_c$) versus temperature curves; and (**c**) the temperature-dependent interface slip length ($2l_y/l_c$) versus temperature curves of 2D C/SiC composite at the vibration frequency of $f = 5$ Hz.

The experimental composite damping (η_c) increases from $\eta_c = 0.007$ at temperature of $T = 136$ °C to the peak value of $\eta_c = 0.0106$ at temperature of $T = 261$ °C and then decreases to $\eta_c = 0.008$ at temperature of $T = 400$ °C. The theoretical predicted composite damping increases from $\eta_c = 0.0048$ at room temperature to the peak value of $\eta_c = 0.0101$ at temperature of $T = 263$ °C and then decreases to $\eta_c = 0.007$ at temperature of $T = 400$ °C. The interface debonding length ($2l_d/l_c$) decreases from $2l_d/l_c = 0.186$ at room temperature to $2l_d/l_c = 0.029$ at temperature of $T = 400$ °C, and the interface slip length ($2l_y/l_c$) decreases from $2l_y/l_c = 0.174$ at room temperature to $2l_y/l_c = 0.029$ at temperature of $T = 400$ °C.

4.1.4. $f = 10$ Hz

The experimental and predicted temperature-dependent composite damping (η_c), interface debonding, and slip length ($2l_d/l_c$, $2l_y/l_c$) versus temperature curves of the 2D C/SiC composite at the vibration frequency of $f = 10$ Hz are shown in Figure 8 and Table 5.
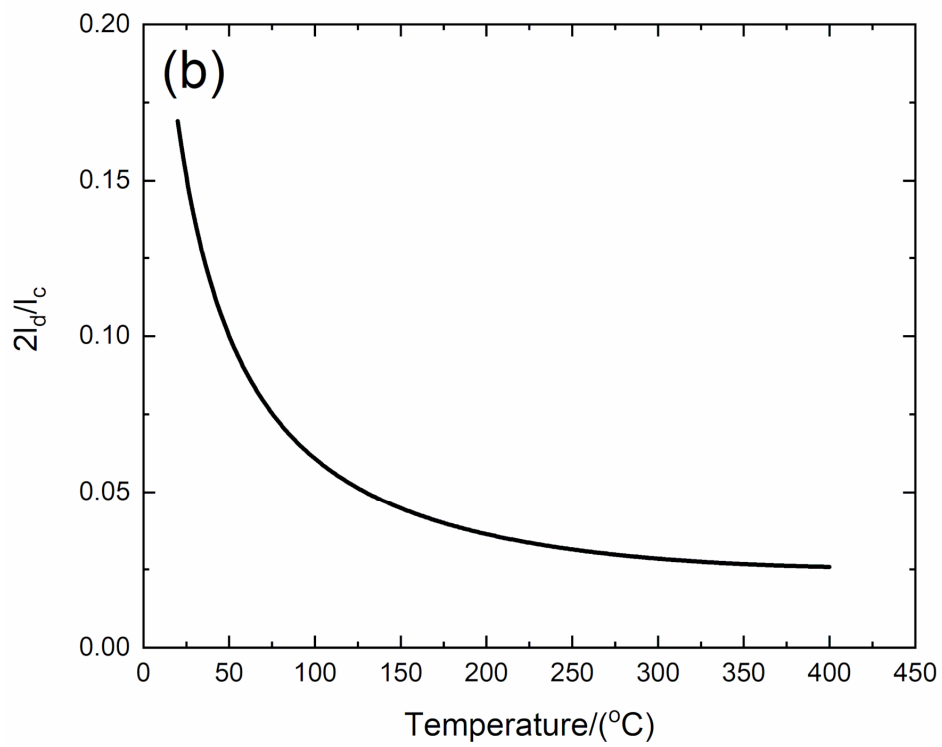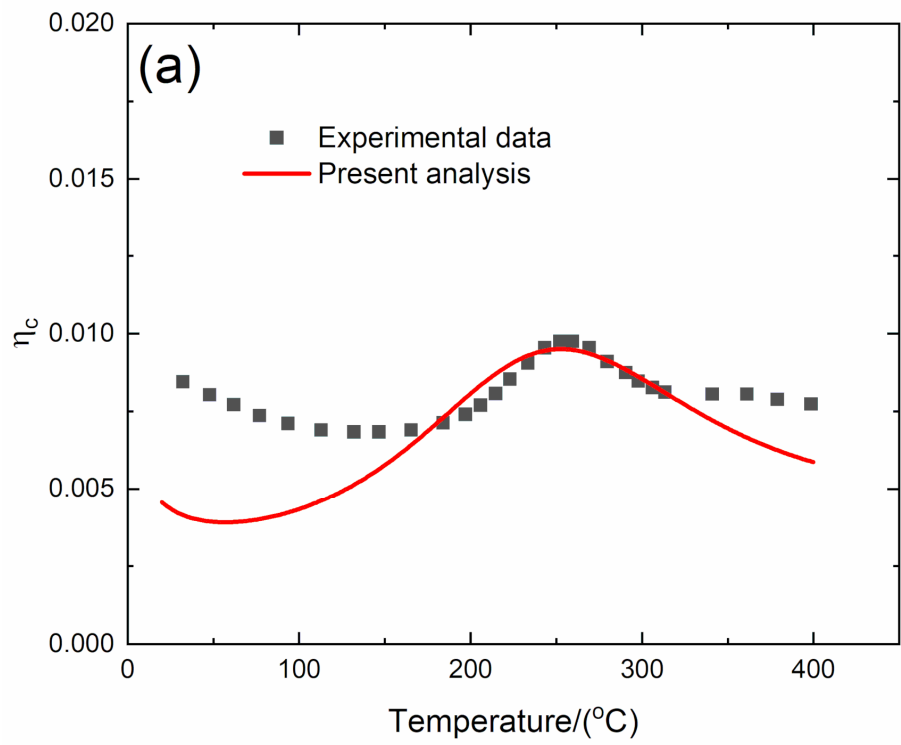
Figure 8. *Cont.*
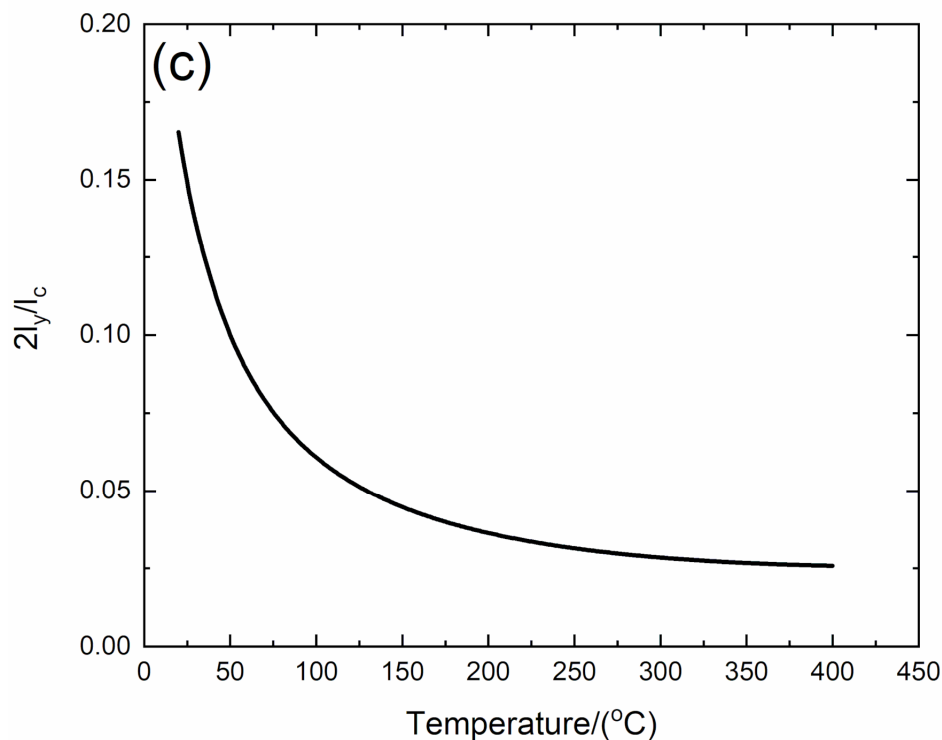
Figure 8. (**a**) Experimental and predicted temperature-dependent composite damping (η_c) versus temperature curves; (**b**) the temperature-dependent interface debonding length ($2l_d/l_c$) versus temperature curves; and (**c**) the temperature-dependent interface slip length ($2l_y/l_c$) versus temperature curves of 2D C/SiC composite at the vibration frequency of f = 10 Hz.

The experimental composite damping (η_c) decreases from η_c = 0.0085 at room temperature to η_c = 0.0068 at temperature of T = 125 °C, then increases to the peak value of η_c = 0.01 at temperature of T = 258 °C, and then decreases to η_c = 0.007 at temperature of T = 400 °C. The theoretical predicted composite damping (η_c) increases from η_c = 0.0045 at room temperature to the peak value of η_c = 0.0095 at temperature of T = 256 °C and then decreases to η_c = 0.0058 at temperature of T = 400 °C. The interface debonding length ($2l_d/l_c$) decreases from $2l_d/l_c$ = 0.169 at room temperature to $2l_d/l_c$ = 0.025 at temperature of T = 400 °C, and the interface slip length ($2l_y/l_c$) decreases from $2l_y/l_c$ = 0.165 at room temperature to $2l_y/l_c$ = 0.0258 at temperature of T = 400 °C.

Under a high loading frequency of f = 10 Hz, the damage mechanism of CMCs including matrix cracking and interface debonding are affected by the loading frequency. Sorensen and Holmes [29] investigated the effect of loading rate on tensile behavior of a SiC/CAS II composite. It was found that the saturation matrix crack spacing increases with loading rate, and dynamic frictional coefficient also increases. However, in the present analysis, the effect of temperature on dynamic loading damage of CMCs (i.e., matrix cracking and interface damage) is not considered. The predicted composite damping is different from the experimental result at low temperature.

4.2. 3D C/SiC Composite

4.2.1. f = 1 Hz

The experimental and predicted temperature-dependent composite damping (η_c), interface debonding, and slip length ($2l_d/l_c$, $2l_y/l_c$) versus temperature curves of the 3D C/SiC composite at the vibration frequency of f = 1 Hz are shown in Figure 9 and Table 6.
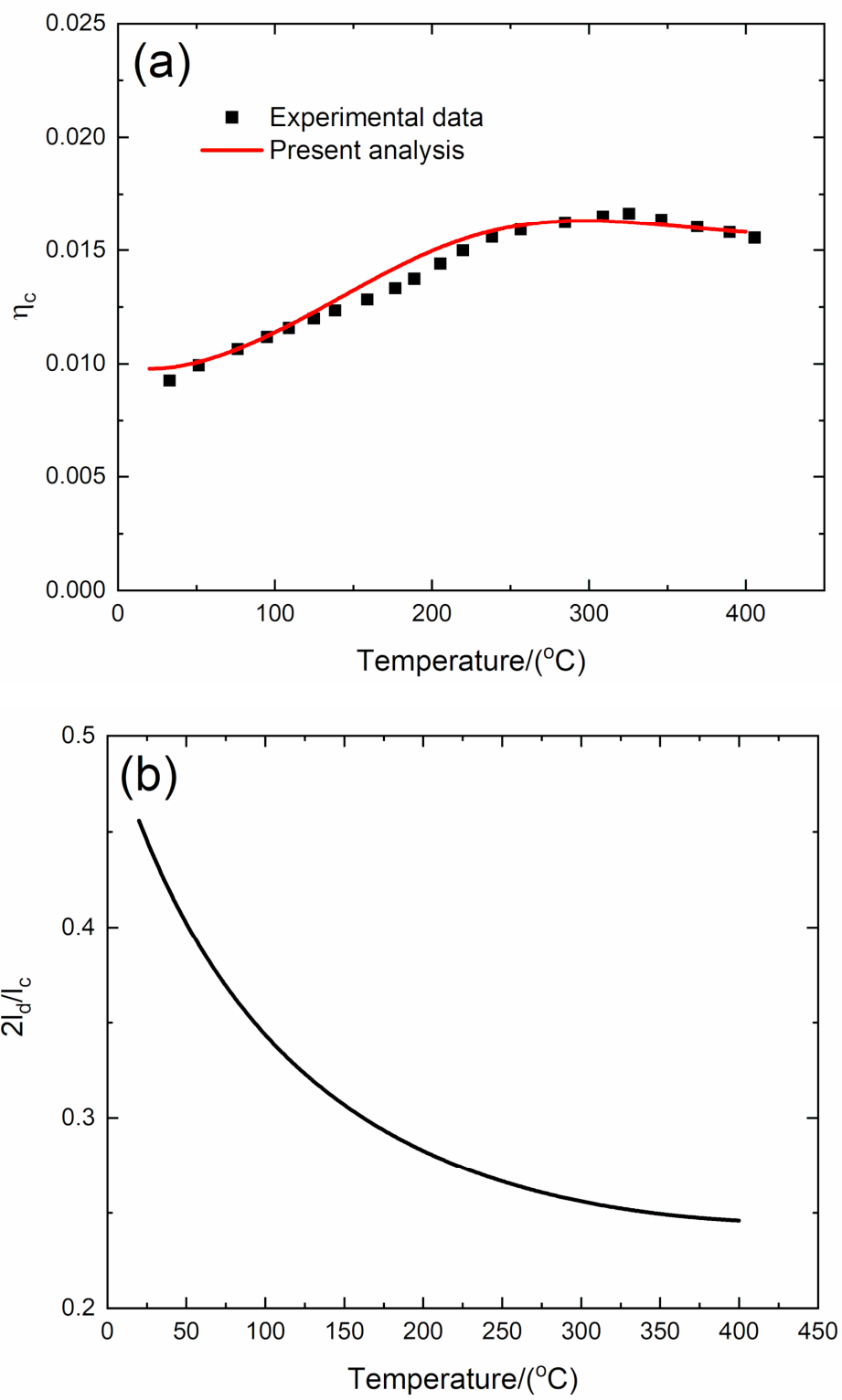
Figure 9. *Cont.*
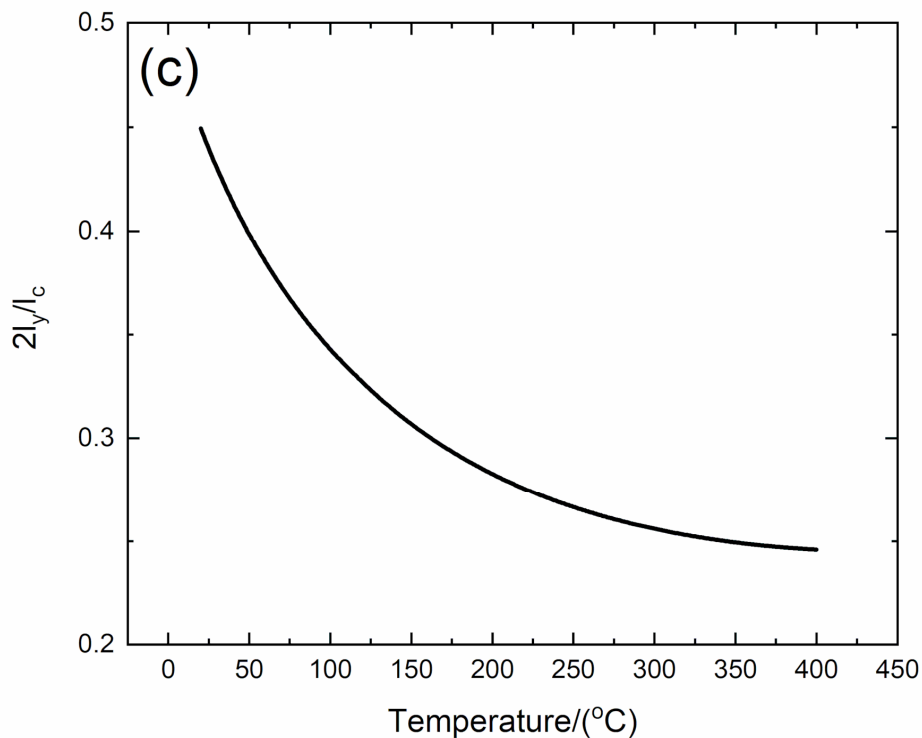
Figure 9. (**a**) Experimental and predicted temperature-dependent composite damping (η_c) versus temperature curves; (**b**) the temperature-dependent interface debonding length ($2l_d/l_c$) versus temperature curves; and (**c**) the temperature-dependent interface slip length ($2l_y/l_c$) versus temperature curves of 3D C/SiC composite at the vibration frequency of f = 1 Hz.

Table 6. Experimental and predicted peak value of composite damping and corresponding temperature of 3D C/SiC composite under the vibration frequencies of f = 1, 2, 5, and 10 Hz at temperature range from room temperature to 400 °C.

Frequency/Hz	Experiment [15]		Theory	
	Peak Damping	Temperature/(°C)	Peak Damping	Temperature/(°C)
1	0.0165	325	0.0163	308
2	0.0135	370	0.0136	360
5	0.0095	300	0.0095	300
10	0.009	295	0.0087	300

The experimental composite damping (η_c) increases from η_c = 0.009 at room temperature to the peak value of η_c = 0.0165 at temperature of T = 325 °C and then decreases to η_c = 0.015 at temperature of T = 400 °C. The theoretical predicted composite damping (η_c) increases from η_c = 0.009 at room temperature to the peak value of η_c = 0.0163 at temperature of T = 308 °C and then decreases to η_c = 0.015 at temperature of T = 400 °C. The interface debonding length ($2l_d/l_c$) decreases from $2l_d/l_c$ = 0.455 at room temperature to $2l_d/l_c$ = 0.245 at temperature of T = 400 °C; and the interface slip length ($2l_y/l_c$) decreases from $2l_y/l_c$ = 0.449 at room temperature to $2l_y/l_c$ = 0.245 at temperature of T = 400 °C.

4.2.2. f = 2 Hz

The experimental and predicted temperature-dependent composite damping (η_c), interface debonding, and slip length ($2l_d/l_c$, $2l_y/l_c$) versus temperature curves of the 3D C/SiC composite at the vibration frequency of f = 2 Hz are shown in Figure 10 and Table 6.
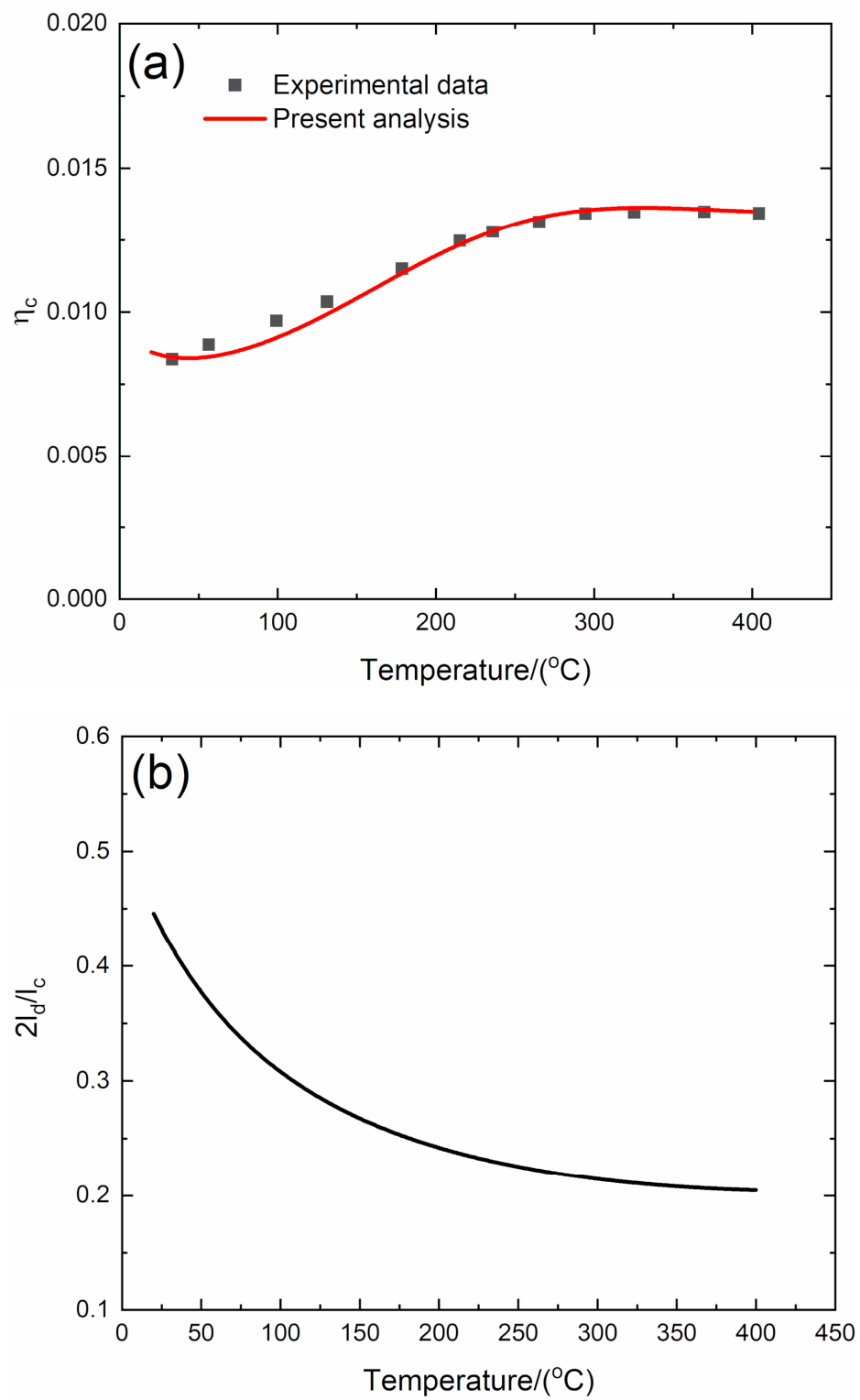
Figure 10. *Cont.*
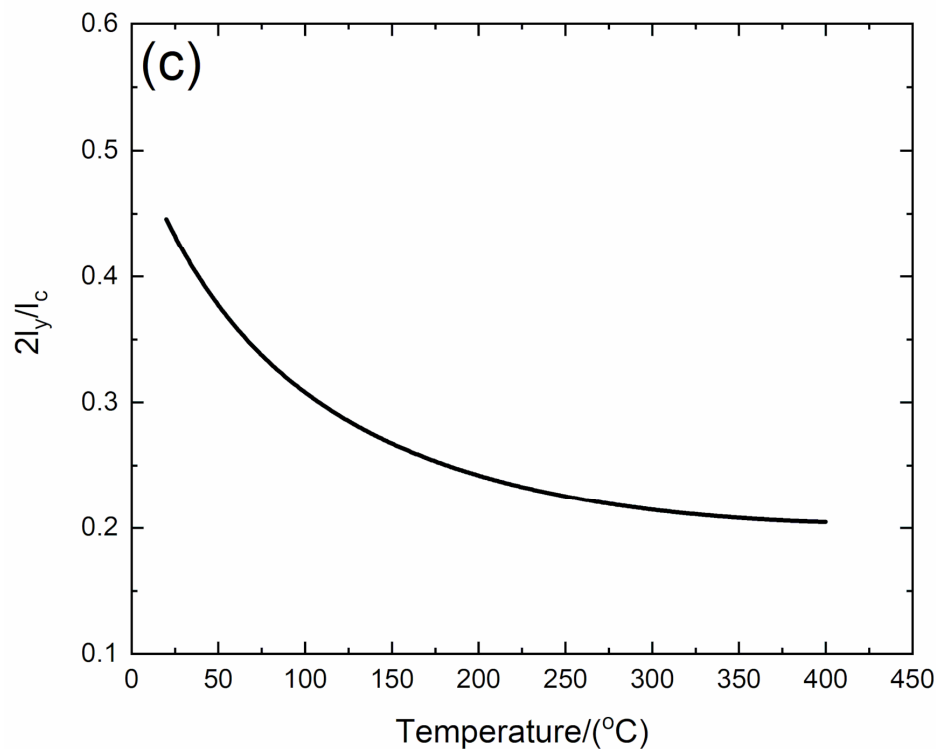
Figure 10. (**a**) Experimental and predicted temperature-dependent composite damping (η_c) versus temperature curves; (**b**) the temperature-dependent interface debonding length ($2l_d/l_c$) versus temperature curves; and (**c**) the temperature-dependent interface slip length ($2l_y/l_c$) versus temperature curves of 3D C/SiC composite at the vibration frequency of f = 2 Hz.

The experimental composite damping (η_c) increases from η_c = 0.0083 at room temperature to the peak value of η_c = 0.0135 at temperature of T = 370 °C and then decreases to η_c = 0.0134 at temperature of T = 400 °C. The theoretical predicted composite damping (η_c) increases from η_c = 0.0086 at room temperature to the peak value of η_c = 0.0136 at temperature of T = 360 °C and then decreases to η_c = 0.0135 at temperature of T = 400 °C. The interface debonding length ($2l_d/l_c$) decreases from $2l_d/l_c$ = 0.445 at room temperature to $2l_d/l_c$ = 0.204 at temperature of T = 400 °C; and the interface slip length ($2l_y/l_c$) decreases from $2l_y/l_c$ = 0.445 at room temperature to $2l_y/l_c$ = 0.204 at temperature of T = 400 °C.

4.2.3. f = 5 Hz

The experimental and predicted temperature-dependent composite damping (η_c), interface debonding, and slip length ($2l_d/l_c$, $2l_y/l_c$) versus temperature curves of the 3D C/SiC composite at the vibration frequency of f = 5 Hz are shown in Figure 11 and Table 6.
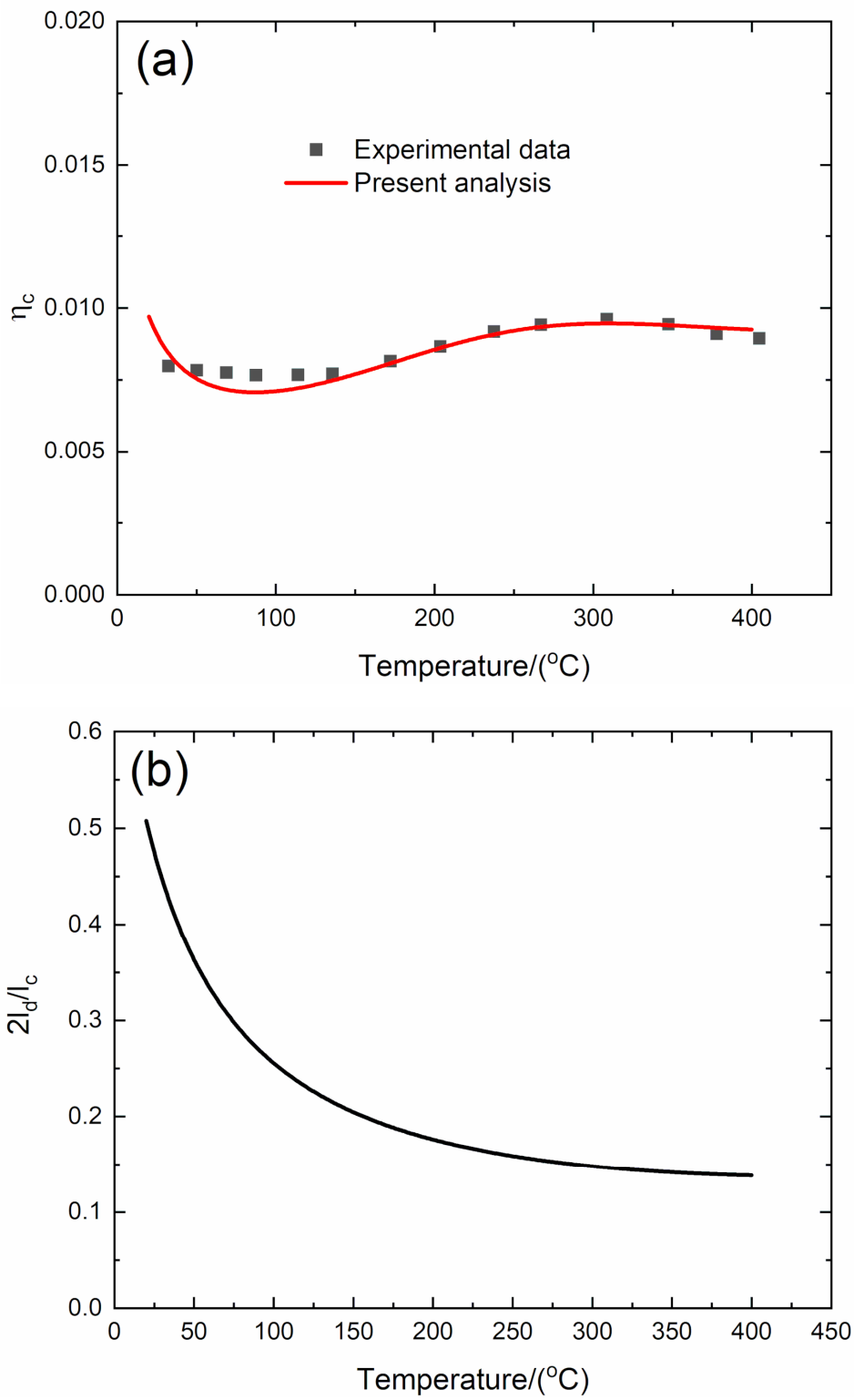
Figure 11. *Cont.*
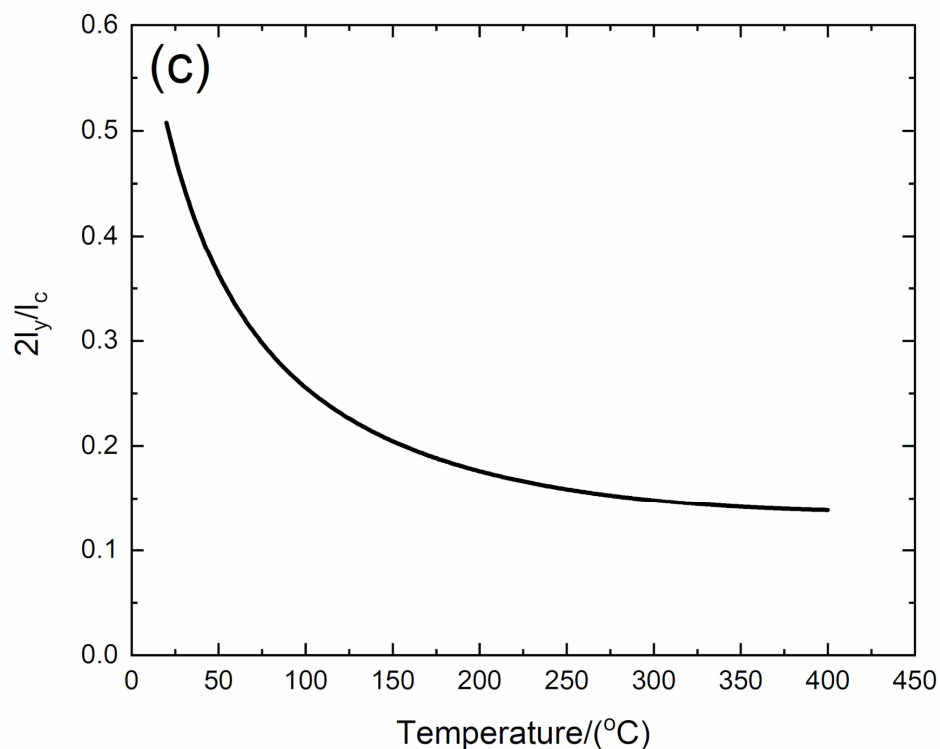
Figure 11. (**a**) Experimental and predicted temperature-dependent composite damping (η_c) versus temperature curves; (**b**) the temperature-dependent interface debonding length ($2l_d/l_c$) versus temperature curves; and (**c**) the temperature-dependent interface slip length ($2l_y/l_c$) versus temperature curves of 3D C/SiC composite at the vibration frequency of $f = 5$ Hz.

The experimental composite damping (η_c) increases from $\eta_c = 0.008$ at room temperature to the peak value of $\eta_c = 0.0095$ at temperature of $T = 300$ °C and then decreases to $\eta_c = 0.009$ at temperature of $T = 400$ °C. The theoretical predicted composite damping (η_c) decreases from $\eta_c = 0.0097$ at room temperature to $\eta_c = 0.007$ at temperature of $T = 86$ °C, then increases to the peak value of $\eta_c = 0.0095$ at temperature of $T = 300$ °C, and then decreases to $\eta_c = 0.0092$ at temperature of $T = 400$ °C. The interface debonding length ($2l_d/l_c$) decreases from $2l_d/l_c = 0.507$ at room temperature to $2l_d/l_c = 0.138$ at temperature of $T = 400$ °C; and the interface slip length ($2l_y/l_c$) decreases from $2l_y/l_c = 0.507$ at room temperature to $2l_y/l_c = 0.138$ at temperature of $T = 400$ °C.

4.2.4. $f = 10$ Hz

The experimental and predicted temperature-dependent composite damping (η_c), interface debonding, and slip length ($2l_d/l_c$, $2l_y/l_c$) versus temperature curves of the 3D C/SiC composite at the vibration frequency of $f = 10$ Hz are shown in Figure 12 and Table 6.
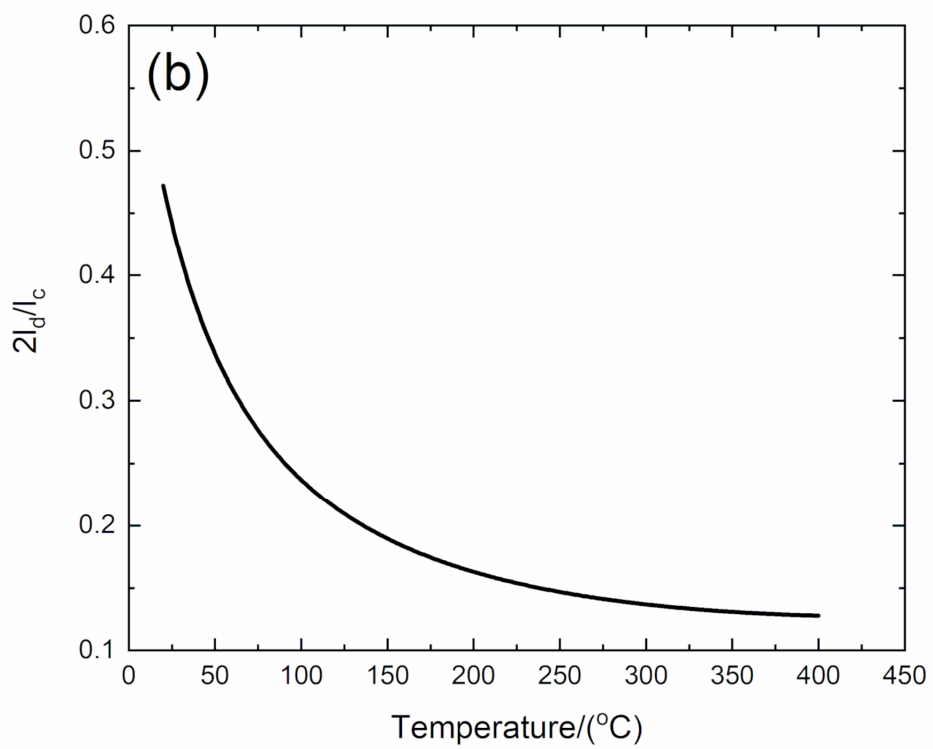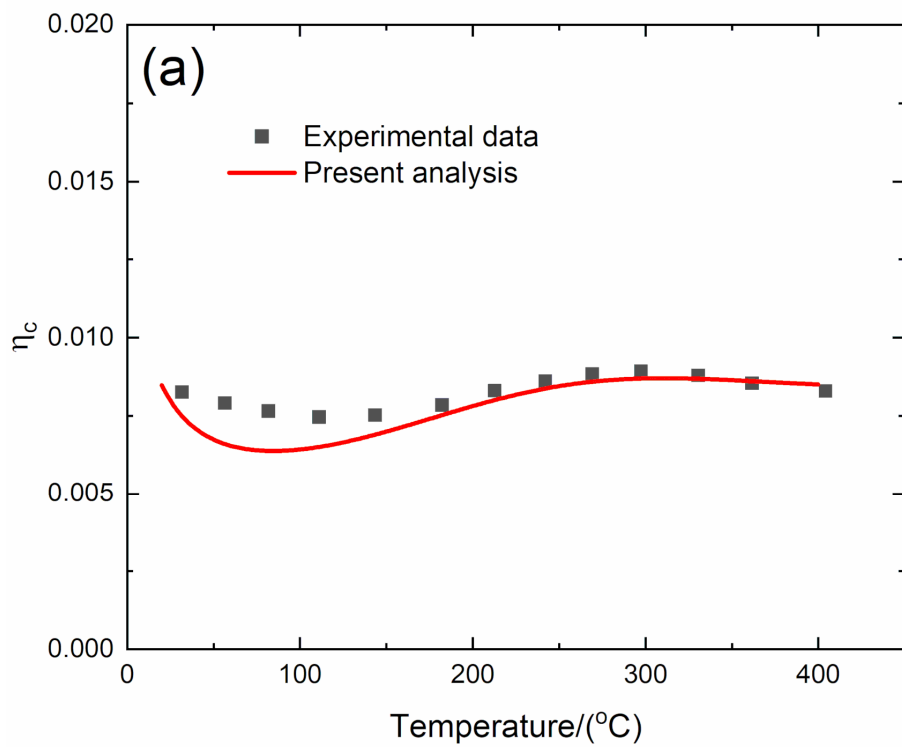
Figure 12. *Cont.*
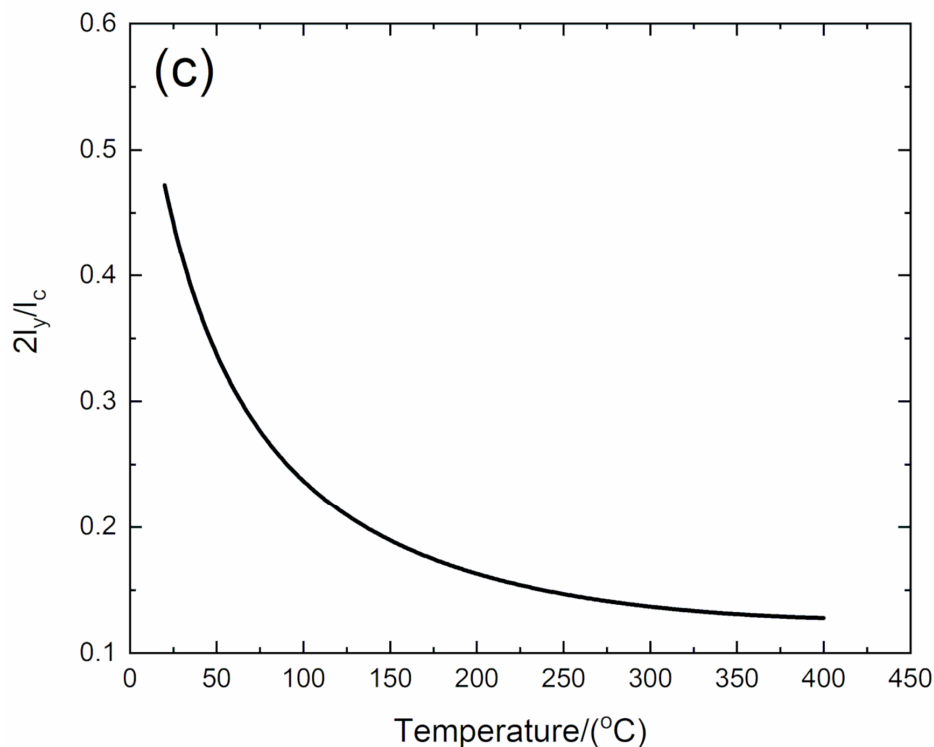
Figure 12. (**a**) Experimental and predicted temperature-dependent composite damping (η_c) versus temperature curves; (**b**) the temperature-dependent interface debonding length ($2l_d/l_c$) versus temperature curves; and (**c**) the temperature-dependent interface slip length ($2l_y/l_c$) versus temperature curves of 3D C/SiC composite at the vibration frequency of $f = 10$ Hz.

The experimental composite damping (η_c) decreases from $\eta_c = 0.0084$ at room temperature to $\eta_c = 0.0075$ at temperature of $T = 125$ °C, then increases to the peak value of $\eta_c = 0.009$ at temperature of $T = 295$ °C, and then decreases to $\eta_c = 0.0084$ at temperature of $T = 400$ °C. The theoretical predicted composite damping (η_c) decreases from $\eta_c = 0.0084$ at room temperature to $\eta_c = 0.0064$ at temperature of $T = 96$ °C, then increases to the peak value of $\eta_c = 0.0087$ at temperature of $T = 300$ °C, and then decreases to $\eta_c = 0.0085$ at temperature of $T = 400$ °C. The interface debonding length ($2l_d/l_c$) decreases from $2l_d/l_c = 0.472$ at room temperature to $2l_d/l_c = 0.127$ at temperature of $T = 400$ °C; and the interface slip length ($2l_y/l_c$) decreases from $2l_y/l_c = 0.472$ at room temperature to $2l_y/l_c = 0.127$ at temperature of $T = 400$ °C.

4.3. Discussion

Due to temperature-dependent material properties and especially the interface properties (i.e., the interface shear stress ($\tau_i(T)$)), the composite damping, interface debonding, and slip state of C/SiC are temperature-dependent. For 2D and 3D C/SiC, the temperature-dependent composite vibration damping increases with temperature to the peak value and then decreases; and the temperature-dependent interface debonding and slip length decrease with temperature. The experimental and predicted composite damping peak values of 2D and 3D C/SiC under vibration frequencies of f = 1, 2, 5, and 10 Hz from room temperature to 400 °C are shown in Tables 5 and 6.

For 2D C/SiC, the composite damping peak value decreases with vibration frequency, i.e., from $\eta_c = 0.019$ at a vibration frequency of f = 1 Hz to $\eta_c = 0.01$ at a vibration frequency of f = 10 Hz, and the corresponding temperature for peak composite damping also decreases, i.e., from $T = 283$ °C at a vibration frequency of f = 1 Hz to $T = 258$ °C at a vibration frequency of f = 10 Hz.

For 3D C/SiC, the composite damping peak value decreases with vibration frequency, i.e., from $\eta_c = 0.0165$ at a vibration frequency of f = 1 Hz to $\eta_c = 0.009$ at a vibration frequency of f = 10 Hz, and the corresponding temperature for peak composite damping also decreases, i.e., from $T = 325\ ^\circ$C at a vibration frequency of f = 1 Hz to $T = 295\ ^\circ$C at a vibration frequency of f = 10 Hz.

For C/SiC, the fiber and matrix damping contributes little to composite damping. However, the frictional dissipated energy caused by frictional slip in the debonding region mainly contributes to the composite damping. For 2D C/SiC, when the vibration frequency increases, the dynamic frictional slip range (i.e., the interface debonding length $2l_d/l_c$ and interface slip length $2l_y/l_c$) decreases, which decreases the energy dissipated through frictional slip and composite damping. For C/SiC with weak interface bonding, the interface debonding occurs when matrix cracking propagates to the fiber/matrix interphase. The frictional slip between the fiber and the matrix or between fiber and fiber causes the energy dissipation, which contributes to the damping of C/SiC. However, when the interface slip range or interface debonding/slip length decreases, the composite damping decreases.

For C/SiC, the composite damping of 2D C/SiC is higher than that of 3D C/SiC, mainly due to the damage mechanisms of matrix cracking and interface debonding. For 3D C/SiC, the fiber volume along the longitudinal loading direction is higher than that of 2D C/SiC, leading to higher matrix cracking density, low interface debonding length, and low composite damping.

5. Conclusions

In this paper, a micromechanical temperature-dependent vibration damping model of a C/SiC composite is developed. The composite damping is divided into damping of the fiber and the matrix and the damping caused by frictional dissipated energy. The relationships between composite damping, composite internal damage, and temperature are established for different material properties and damage states. The experimental temperature-dependent damping of 2D and 3D C/SiC are predicted for different vibration frequencies.

(1) For C/SiC, the temperature-dependent composite vibration damping increases with temperature to the peak value and then decreases, and the temperature-dependent interface debonding and slip length decrease with temperature.

(2) For C/SiC, when the vibration frequency increases, the dynamic frictional slip range decreases, which decreases the energy dissipated through frictional slip and composite damping.

(3) For 3D C/SiC, the fiber volume along the longitudinal loading direction is higher than that of 2D C/SiC, leading to higher matrix cracking density, low interface debonding length, and low composite damping.

(4) When fiber volume and interface debonding energy increase, the peak value of composite damping and the corresponding temperature both decrease.

(5) When matrix crack spacing and steady-state interface shear stress increase, the peak value of composite damping decreases, and the corresponding temperature for peak damping changes a little.

Conflicts of Interest: The author declares no conflict of interest. The funders had no role in the design of the study; in the collection, analyses, or interpretation of data; in the writing of the manuscript, or in the decision to publish the results.

Data Availability: The data used to support the findings of this study are available from the paper.

Nomenclature

η	composite damping
η_a	composite damping of CMCs without damage
η_b	composite damping of CMCs with damage
η_c	total composite damping of CMCs
U_d	dissipated energy density per cycle
U	maximum strain energy density per cycle
σ	stress amplitude of vibration stress
σ_c	vibration stress
ω	vibration frequency
r_f	fiber radius
V_f	fiber volume
V_m	matrix volume
E_f	fiber elastic modulus
E_m	matrix elastic modulus
$\bar{E}_m$	effective matrix elastic modulus
E_c	composite elastic modulus
l_d	interface debonding length
l_y	interface counter slip length
l_z	interface new slip length
l_c	matrix crack spacing
U_{d_u}	dissipated energy density upon unloading
U_{d_r}	dissipated energy density upon reloading
U_f	fiber strain energy density per cycle
U_m	matrix strain energy density per cycle
ξ_d	interface debonding energy
ρ	shear-lag model parameter
σ_{fo}	fiber axial stress in the bonding region
σ_{mo}	matrix axial stress in the bonding region
α_{rf}	fiber radial thermal expansional coefficient
α_{lf}	fiber axial thermal expansional coefficient
α_{rm}	matrix radial thermal expansional coefficient
α_{lm}	matrix axial thermal expansional coefficient
α_{lc}	composite axial thermal expansional coefficient
ΔT	temperature difference between testing and fabricated temperature
τ_i	interface shear stress
τ_0	steady-state interface shear stress
μ	interface frictional coefficient

References

1. Naslain, R. Design, Preparation and properties of non-oxide CMCs for application in engines and nuclear reactors: An overview. *Compos. Sci. Technol.* **2004**, *64*, 155–170. [CrossRef]
2. Li, L.B. Durability of ceramic-matrix composites. *Elsevier* **2020**. [CrossRef]
3. Min, J.B.; Harris, D.L.; Ting, J.M. Advances in ceramic matrix composite blade damping characteristics for aerospace turbomachinery applications. In Proceedings of the 52nd AIAA/ASME/ASCE/AHS/ASC Structures, Structural Dynamics and Materials Conference, Denver, Colorado, 4–7 April 2011. [CrossRef]
4. Momon, S.; Moevus, M.; Godin, N.; R'Mili, M.; Reynaud, P.; Fantozzi, G.; Fayolle, G. Acoustic emission and lifetime prediction during static fatigue tests on ceramic-matrix-composite at high temperature under air. *Compos. Part A* **2010**, *41*, 913–918. [CrossRef]
5. Zhang, J.; Perez, R.J.; Lavernia, E.J. Documentation of damping capacity of metallic ceramic and metal-matrix composite materials. *J. Mater. Sci.* **1993**, *28*, 2395–2404. [CrossRef]
6. Chandra, R.; Singh, S.P.; Gupta, K. Damping studies in fiber-reinforced composites—A review. *Compos. Struct.* **1999**, *46*, 41–51. [CrossRef]

7. Birman, V.; Byrd, L.W. Damping in ceramic matrix composites with matrix cracks. *Int. J. Solids Struct.* **2003**, *40*, 4239–4256. [CrossRef]
8. Melo, J.D.; Radford, D.W. Time and temperature dependence of the viscoelastic properties of CFRP by dynamic mechanical analysis. *Compos. Struct.* **2005**, *70*, 240–253. [CrossRef]
9. Patel, R.K.; Bhattacharya, B.; Basu, S. A finite element based investigation on obtaining high material damping over a larger frequency range in viscoelastic composites. *J. Sound Vib.* **2007**, *303*, 753–766. [CrossRef]
10. Sato, S.; Serizawa, H.; Araki, H.; Node, T.; Kohyama, A. Temperature dependence of internal friction and elastic modulus of SiC/SiC composites. *J. Alloy. Compd.* **2003**, *355*, 142–147. [CrossRef]
11. Gowayed, Y.; Ojard, G.; Santhosh, U.; Jefferson, G. Modeling of crack density in ceramic matrix composites. *J. Compos. Mater.* **2015**, *49*, 2285–2294. [CrossRef]
12. Birman, V.; Byrd, L.W. Effect of matrix cracks on damping in unidirectional and cross-ply ceramic matrix composites. *J. Compos. Mater.* **2002**, *36*, 1859–1877. [CrossRef]
13. Zhang, Q.; Cheng, L.F.; Wang, W.; Wei, X.; Zhang, L.T.; Xu, Y.D. Effect of interphase thickness on damping behavior of 2D C/SiC composites. *Mater. Sci. Forum* **2007**, *546–549*, 1531–1534. [CrossRef]
14. Hong, Z.L.; Cheng, L.F.; Zhao, C.N.; Zhang, L.T.; Wang, Y.G. Effect of oxidation on internal friction behavior of C/SC composites. *Acta Mater. Compos. Sin.* **2013**, *30*, 93–100.
15. Wang, W. Study on Damping Capacity of C/SiC Composites. Master's Thesis, Northwestern Polytechnical University, Xi'an, China, 2005.
16. Zhang, Q.; Cheng, L.; Wang, W.; Zhang, L.; Xu, Y. Effect of SiC coating and heat treatment on damping behavior of C/SiC composites. *Mater. Sci. Eng. A* **2008**, *473*, 254–258. [CrossRef]
17. Holmes, J.W.; Cho, C. Experimental observation of frictional heating in fiber-reinforced ceramics. *J. Am. Ceram. Soc.* **1992**, *75*, 929–938. [CrossRef]
18. Li, L.B. Modeling fatigue hysteresis behavior of unidirectional C/SiC ceramic-matrix composites. *Compos. Part B* **2014**, *66*, 466–474. [CrossRef]
19. Li, L.B. Modeling matrix multicracking development of fiber-reinforced ceramic-matrix composites considering fiber debonding. *Int. J. Appl. Ceram. Technol.* **2019**, *16*, 97–107. [CrossRef]
20. Li, L.B. Time-dependent damage and fracture of fiber-reinforced ceramic-matrix composites at elevated temperatures. *Compos. Interfaces* **2019**, *26*, 963–988. [CrossRef]
21. Li, H.Q. Analysis of Vibration and Damage Test of Ceramic Matrix Composites Structure. Master's Thesis, Nanchang Hongkong University, Nanchang, China, 2019.
22. Kyriazoglou, C.; Page, B.H.; Guild, F.J. Vibration damping for crack detection in composite laminates. *Compos. Part A* **2004**, *35*, 945–953. [CrossRef]
23. Zhang, Z.; Hartwig, G. Relation of damping and fatigue damage of unidirectional fiber composites. *Int. J. Fatigue* **2002**, *24*, 713–718. [CrossRef]
24. Sauder, C.; Lamon, J.; Pailler, R. The tensile behavior of carbon fibers at high temperatures up to 2400 °C. *Carbon* **2004**, *42*, 715–725. [CrossRef]
25. Snead, L.L.; Nozawa, T.; Katoh, Y.; Byun, T.S.; Kondo, S.; Petti, D.A. Handbook of SiC properties for fuel performance modeling. *J. Nucl. Mater.* **2007**, *371*, 329–377. [CrossRef]
26. Pradere, C.; Sauder, C. Transverse and longitudinal coefficient of thermal expansion of carbon fibers at high temperatures (300–2500K). *Carbon* **2008**, *46*, 1874–1884. [CrossRef]
27. Reynaud, P.; Douby, D.; Fantozzi, G. Effects of temperature and of oxidation on the interfacial shear stress between fibers and matrix in ceramic-matrix composites. *Acta Mater.* **1998**, *46*, 2461–2469. [CrossRef]
28. Wang, R.Z.; Li, W.G.; Li, D.Y.; Fang, D.N. A new temperature dependent fracture strength model for the ZrB$_2$-SiC composites. *J. Eur. Ceram. Soc.* **2015**, *35*, 2957–2962. [CrossRef]
29. Sorensen, B.F.; Holmes, J.W. Effect of loading rate on the monotonic tensile behavior of a continuous-fiber-reinforced glass-ceramic matrix composite. *J. Am. Ceram. Soc.* **1996**, *79*, 313–320. [CrossRef]